Imperial College London


**IMPERIAL COLLEGE LONDON**

Faculty of Engineering

*Department of Civil and Environmental Engineering*

# A hybrid model for predicting coastal flooding

**N.S. Vinay Krishna Rayudu**

2019-2020

Submitted in fulfilment of the requirements for the MSc and the Diploma of Imperial College London

## DECLARATION OF OWN WORK

**Declaration:**

This submission is my own work. Any quotation from, or description of, the work of others is acknowledged herein by reference to the sources, whether published or unpublished.

Signature: N.S. Vinay Krishna Rayudu

# Abstract

A large part of the world population resides in coastal regions. The rise in sea levels due to global warming and the increase in the frequency of extreme events in coastal areas poses a serious threat to them in the form of flooding. This warrants the availability of a fast and accurate computational solver to predict coastal flooding. The complex coastal processes make it difficult to model the phenomenon numerically. Further, numerical models often have a trade-off between speed and accuracy.

In this study, a hybrid computational model based on shallow water equations is proposed. The computational domain is divided into three zones based on significant physical processes. In the first zone, deep water waves start propagating into the domain and one layer non-hydrostatic shallow water equations are implemented. As the waves propagate onto the beach slope they start to steepen and break, marking the first division of the computational domain. In the second zone, hydrostatic shallow water equations are implemented which allows the wave to transform into a bore-like shape to simulate the effects of wave breaking and compensate for the low vertical resolution. The next division is made where the waves over-top the sea defence and flood the coastal region. Here, the flow behaviour is in the form of non-dispersive fluxes and a hydrostatic shallow water model without advection is implemented. Further, to improve the accuracy of the results, a set-up correction is implemented.

The proposed numerical model is developed in Python3 in a modular fashion. The language is selected because it is modern and allows for easy development and coupling with other models in the future. The model is validated for various cases with an existing robust model SWASH and is found to produce accurate results.

Further work to be conducted on this involves the implementation of parallel processing and methods to resolve irregular bathymetries. The fully developed model will be able to perform real-time flood estimates, nearshore modelling, and flood risk analysis in national scales.

# Acknowledgements

I would like to start by thanking my supervisor Dr. Ioannis Karmpadakis for his able guidance and support. I would like the academics, scholars, and students from the IC-COAST group of the Civil Fluid Mechanics Community at Imperial, for the various discussions that provided valuable insights which improved my own project and further, the critical comments on my project itself. The weekly discussions were something to look for every Thursday. I would like Tammo for initial help with SWASH scripts and Guillaume for proofreading the whole report. Further, I appreciate the timely responses by the ICT team regarding HPC related issues. I end this by thanking my family, friends and classmates for their support.

N.S. Vinay Krishna Rayudu,
Imperial College London, August 2020.

# Contents

# 1 Introduction

## 1.1 Research motivation

Coastal areas have always attracted people due to the availability of resources and logistical connectivity acting as access points for marine trade and transport. Furthermore, they are densely populated than the hinterland and exhibit higher rates of population growth and urbanization. Coastal areas are exposed to a range of coastal hazards including storms, and sea-level rise which pose risk in the form of flooding. Coastal flooding causes loss of life and severe losses to population and property. This warrants the development of tools to predict coastal flooding. The developed tools can be used be in flood risk analysis, early warning systems, and development of coastal defenses.

*Figure 1: The flooding of New Orleans, caused by Hurricane Katrina in 2005, illustrates the vulnerability of cities that are highly dependent on coastal defenses. Photo: NOAA from (Wikipedia, the free encyclopedia, 2005)*

## 1.2 Research approach

The main objective of this thesis is to provide a fast computational model for predicting coastal flooding. Unlike traditional models that almost fully resolve all the physics included in the approach over the whole domain. This thesis provides a hybrid model where different sets of governing equations are applied in the com-

putational model on a zone by zone basis. In essence, the computational domain is divided into three zones based on significant physical processes in each zone(see figure 5).

First, an appropriate numerical model is found for each zone. For, offshore and near-shore the equations from a single layer SWASH(Zijlema et al., 2011) model are adapted and a multiple time-step method was adapted to solve them. It is then validated without bifurcating the zones 1 and 2. For, the over-topped zone, the model need not capture any coastal phenomenon as it only propagates over-topped water which are non-dispersive fluxes.

Once the primary hydrostatic and non-hydrostatic models are selected, a parametric depth model for bifurcation of the domain was decided. The non-hydrostatic pressure components of the equations will be barred from computation in zone 2. The reason for this is due to the low vertical resolution of one layer, the non-hydrostatic pressure must be switched off after onset breaking to ensure that the wave transforms into a bore-like shape to simulate the effects of wave breaking. Then, as the model is to be used for predicting coastal flooding, the set-up is corrected using a parametric formulation.

In summary, the hybrid model will three zones which zone 1 in the offshore boundary, zone 2 which is from the bifurcation depth to the over-topping point, and zone 3 the flood propagation zone. The bifurcation point is derived by parametrizing the breaking depth using the wave saturation approach. A set-up parametrization is attempted as there might be a need for set-up correction.

## 1.3 Readers guide

This thesis starts with the background chapter(2). It starts with the basic definitions of key coastal processes that drive coastal flooding. Furthermore, it presents an overview of the ways to numerically model these processes and the similarities

between them.

The next chapter is the methodology chapter(3). This chapter starts by explaining and justifying the zonal approach adopted in the current project for the development of the hybrid model. Next, the numerical methods implemented for the non-hydrostatic model based on a single layer SWASH(Zijlema *et al.*, 2011) equations is demonstrated and validated. After that, parametric models were derived for the bifurcation depth between zones 1 and 2 and the maximum wave set-up. Furthermore, the hydrostatic model for flood propagation by Bates *et al.* (2010) is also demonstrated and validated. The chapter ends with the description of the numerical implementation flooding and drying at the dry-wet boundary.

It is then followed by the results and discussion chapter(4). This chapter starts with comparison of the full non-hydrostatic model with the SWASH model and then the hybrid model is compared with the full non-hydrostatic model to assess whether the derived set-up corrected is to be implemented. After that, a range of over-topping simulations by the hybrid model are compared with the SWASH model to observe the level of agreement between the models. The chapter ends with a thorough discussion of the above results. Finally, simulations of a basic bar profile are compared with SWASH simulations with different bifurcation points.

Finally, the report is concluded in the conclusion chapter(5). It consists of closing remarks about the current developed model and the future improvements that should be included to make the model complete and versatile.

# 2 Background

This chapter starts with the definition of key coastal processes that drive coastal flooding and ends with a review of existing methods that model these processes. The background information on the coastal processes will be limited to basic definitions. For any further information on the mentioned phenomena, the reader is directed to two standard textbooks Svendsen (2006) and Dean & Dalrymple (1991).

## 2.1 Coastal Processes

### Evolution of a typical wave

A typical wave is generated in the intercontinental shelf region in figure 2, where it can be considered as a deep water wave. As the wave propagates towards the shore, it encounters a beach slope resulting in a decrease in water depth as is propagates towards the shore. This is where the first wave transformation of shoaling happens. Shoaling results in an increase in wave height and a simultaneous decrease in wavelength. This phenomenon is only significant in short or high frequency waves and low frequency or long waves are almost unaffected by this phenomenon.

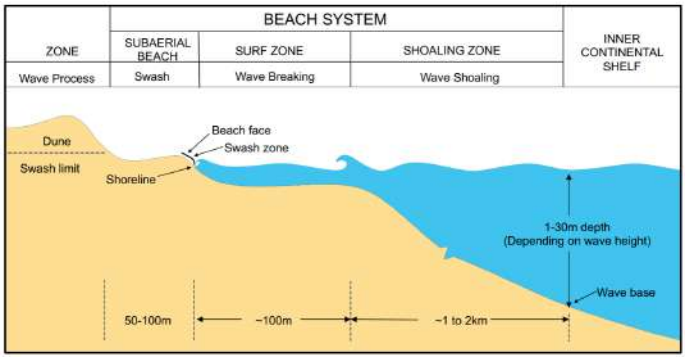


*Figure 2: A typical beach profile from Karmpadakis (2020).*

At a particular depth, further steepening in waves would no longer result in a physically possible wave and here the waves break. The zone at which most waves break is identified as the surf zone and is prone to recreational activities. These broken waves travel further towards the shore where there reach the swash zone. The swash zone is the dynamic region that switches between wet and dry states and is one of

the most difficult regions to model since the domain has to switch as wet and dry numerically.

## Changes in water level near shore

It is to be noted that all the aforementioned phenomena are assumed to occur about the mean sea level. However, there are few additional effects like wave set-up, storm surges, tides, and sea-level rise which change the mean level at which coastal processes occur at a local level(see figure 3).

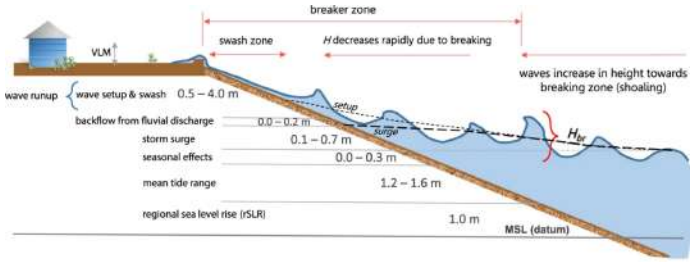


*Figure 3: Change to mean sea level near shore from Barnard* et al. *(2019).*

The local sea-level rise is the by-product of global warming and results in a permanent rise in the mean sea level locally. This is then topped by seasonal changes in sea level. The next effect is the tidal elevation which is due to the gravitational pull of celestial bodies. The tidal elevations are long-range motions which are able to dry hundreds of meters of land in low tide and similarly flood large areas during high tide.

Storm surges are the large-scale increase in surface elevation due to the presence of high-velocity winds during storms. The high wind speeds exert large shear stresses on the water surface, resulting in a piling up of water near the coast and the low atmospheric pressures associated with storms may further amplify this.

Wave set-up is based on radiation stresses. These so-called radiation stress are cross-shore and alongshore gradients in wave-induced momentum fluxes. They are responsible for the rise in mean water levels and generate currents as a result of the body forces caused by them.

### Infra-gravity waves

The information in this section is obtained from Rijnsdorp (2011). Infra-gravity waves are surface gravity waves with low frequencies between 0.005Hz - 0.05Hz and relatively small amplitudes compared to short waves. They can be classified into two types, bound infra-gravity waves, and free infra-gravity waves. The bound infra-gravity waves are generated in deep water and reach the shore a part of the wave group structure. The free infra-gravity waves are generated in the coastal region by two mechanisms.

The first mechanism is the release of bound infra-gravity waves in the surf zone and the second mechanism infra-gravity waves of generation is due to the strong gradients in radiation stresses during wave breaking. Further, the infra-gravity waves can be categorized into leaky and edgy waves. Leaky waves are the infra-gravity which are reflected from the shore and keep propagating away from shore. Edgy waves are in an endless cycle of being reflected by the shore and get heavily refracted to the point where start travelling towards the shore again and in a way, they are trapped near shore.

## 2.2 Coastal modelling

To model/simulate any fluid mechanic problem with the highest accuracy one must use the full Navier-Stokes equations and is usually called a direct numerical simulation(DNS). However, DNS is highly impractical due to its high computational costs and runtimes. To simulate a few seconds of real-time using DNS would take a few days even on the powerful computers today. So, scientists and engineers have simplified the Navier-Stokes equations using several assumptions valid for the problem/scenario they simulate. The common simplification of this sort in coastal modelling is the depth averaging of Navier-Stokes equations. These equations can be simplified primarily into three types, which are non-linear shallow water equations, Boussinesq-type equations, and Serre or Green & Naghdi equations.

These models can be classified based on their dispersion and non-linear properties. The Boussinesq-type equations are weakly dispersive and weakly nonlinear. The Serre-type equations are weakly dispersive and fully nonlinear. The non-linear shallow water equations are non-linear and non-dispersive. Since this project aims to achieve speed by reducing the complexity of the model, non-linear shallow water equations were chosen for modelling.

First, before we comment on details, the shallow water equations and the SWASH equations which are the shallow water equations with a non-hydrostatic pressure balance term are explained in the following two sections. They are then followed by the additional comments.

### 2.2.1 The Shallow-Water Equations

The information in this section is obtained from Van Engelen (2016).

The Shallow-Water equations are derived by depth integrating the 3D Navier-Stokes equations. This is done under the assumption that the horizontal scale of the flow is much greater than the vertical scale of the flow. Typical flows where this assumption is valid is tidal waves, tsunami waves and river flood flows. Under this assumption, it can be showed the vertical momentum equation in the Navier-Stokes equations can be reduced to a hydrostatic pressure balance equation. Additionally, assuming the fluid to be incompressible and depth integrating the Navier-Stokes Equations we end up with the 2D shallow water equations which are given as follows:

$$\frac{\partial \zeta}{\partial t} + \frac{\partial hu}{\partial x} + \frac{\partial hv}{\partial y} = 0 \tag{1}$$

$$\frac{\partial u}{\partial t} + u\frac{\partial u}{\partial x} + v\frac{\partial u}{\partial y} = -g\frac{\partial \zeta}{\partial x} + fv + \nu_h\left(\frac{\partial^2 u}{\partial x^2} + \frac{\partial^2 u}{\partial y^2}\right) - \frac{\tau_{b,x}}{\rho_0 h} + \frac{\tau_{w,x}}{\rho_0 h} - \frac{1}{\rho_0}\frac{\partial P_{atm}}{\partial x} \tag{2}$$

$$\frac{\partial v}{\partial t} + u\frac{\partial v}{\partial x} + v\frac{\partial v}{\partial y} = -g\frac{\partial \zeta}{\partial y} - fu + \nu_h\left(\frac{\partial^2 v}{\partial x^2} + \frac{\partial^2 v}{\partial y^2}\right) - \frac{\tau_{b,y}}{\rho_0 h} + \frac{\tau_{w,y}}{\rho_0 h} - \frac{1}{\rho_0}\frac{\partial P_{atm}}{\partial y} \tag{3}$$

$$h = \zeta + d, \quad \overrightarrow{\tau_w} = \rho_{air} c_d \overrightarrow{U_{10}} \left|\overrightarrow{U_{10}}\right|, \quad \overrightarrow{\tau_b} = \rho_0 c_f \vec{U}|\vec{U}|, \quad f = 2|\Omega|\sin\phi$$

Where, equation 1 is the global continuity equation and equations 2, 3 are global momentum equations. The 2D shallow water equations from a non-linear coupled system with $\zeta$, u and v. where $t$ is the time; $u$ and $v$ are the depth-averaged flow velocities in $x$ and $y$ -direction respectively; $\zeta$ is the free-surface height; h is the water-depth; d is the bottom level defined negative downward (see figure 4); $\rho_0$ is the water density; f is the Coriolis parameter; g the gravitational acceleration; $P_{atm}$ the atmospheric pressure; $\nu_h$ the effective horizontal kinematic viscosity; $\tau_b$ the bottom shear stress and $\tau_w$ the wind shear stress. The bottom and wind shear stresses can be approximated using quadratic friction laws with empirical drag and friction coefficients.

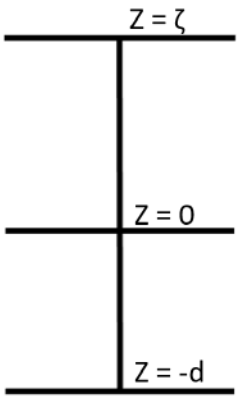


*Figure 4: Definition of bottom depth(d), mean water level and surface elevation($\zeta$).*

Assuming the flow to be 1D in x-direction i.e.$v = 0$ and $\frac{\partial}{\partial y} = 0$. Dropping out Coriolis forcing and friction is taken into account as a body force, then $\nu_h$ can be assumed as zero. Neglecting external forcing due to wind stress and atmospheric pressure gradients. The 2D swallow-water equations can be reduced to the following 1D equations for conservation of mass and momentum:

$$\frac{\partial \zeta}{\partial t} + \frac{\partial hu}{\partial x} = 0 \tag{4}$$

$$\frac{\partial u}{\partial t} + u\frac{\partial u}{\partial x} = -g\frac{\partial \zeta}{\partial x} - \frac{\tau_b}{\rho_0 h} \tag{5}$$

Replacing the bottom friction term with empirical friction based term and Substituting the Manning bed friction coefficient ($n$) for the dimensionless friction coefficient($C_f$

) with:

$$C_f = \frac{gn^2}{h^{1/3}} \tag{6}$$

$$\tau_b = \rho_0 C_f \vec{U}|\vec{U}| \tag{7}$$

Integrating equation 4 over the width(B) and integrating equation 5 over the cross-sectional area ($A_s$) and defining volumetric flow rate as $Q = u.A_s$. We get a system of equations also known as Saint-Venant equations (de Saint-Venant, 1871):

$$B\frac{\partial \zeta}{\partial t} + \frac{\partial Q}{\partial x} = 0 \tag{8}$$

$$\underbrace{\frac{\partial Q}{\partial t}}_{inertia} + \underbrace{\frac{\partial}{\partial s}\left[\frac{Q^2}{A_s}\right]}_{advection} = \underbrace{-gA_s\frac{\partial \zeta}{\partial s}}_{free-surface\ \ gradient} - \underbrace{\frac{gn^2Q|Q|}{R^{4/3}A_s}}_{bottom friction} \tag{9}$$

Where, $R = A_s/P$ is the hydraulic radius and $P$ is the wetted perimeter. This is used in the manning formulation instead of water depth $h$ as the friction is due to the whole wetted are of the channel.

### 2.2.2 SWASH: Simulation of WAves till SHore

The information in this section is obtained from Zijlema *et al.* (2011), Stelling & Zijlema (2003), and Costanza & Carlo (2016).

SWASH is a computational model for simulating non-hydrostatic free surface flows in one and two horizontal dimensions. The governing equations are the non-linear shallow water equations including non-hydrostatic pressure balance. Although SWASH uses the depth averaged Navier-Stokes equations, it uses a multilayer approach to compensate for this and resolve the dispersive effects of the waves. Since, the aim of the project is to develop a simple model, only 1-layer SWASH equations are presented here.

$$\frac{\partial \zeta}{\partial t} + \frac{\partial hu}{\partial x} + \frac{\partial hv}{\partial y} = 0 \tag{10}$$

$$\frac{\partial u}{\partial t} + u\frac{\partial u}{\partial x} + v\frac{\partial u}{\partial y} = -g\frac{\partial \zeta}{\partial x} - \frac{1}{h}\int_{-d}^{\zeta}\frac{\partial q}{\partial x}dz - C_f\frac{u\sqrt{u^2+v^2}}{h} + \frac{1}{h}\left(\frac{\partial h\tau_{xx}}{\partial x} + \frac{\partial h\tau_{xy}}{\partial y}\right) \tag{11}$$

$$\frac{\partial v}{\partial t} + u\frac{\partial v}{\partial x} + v\frac{\partial v}{\partial y} = -g\frac{\partial \zeta}{\partial y} - \frac{1}{h}\int_{-d}^{\zeta}\frac{\partial q}{\partial y}dz - C_f\frac{v\sqrt{u^2+v^2}}{h} + \frac{1}{h}\left(\frac{\partial h\tau_{yx}}{\partial x} + \frac{\partial h\tau_{yy}}{\partial y}\right) \tag{12}$$

where $t$ is time, $x$ and $y$ are located at the still water level and the z-axis pointing upwards, $\zeta$ is the surface elevation measured from the still water level, d is the still water depth, or downward measured bottom level, $h = \zeta + d$ is the water depth, or total depth, $u$ and $v$ are the depth-averaged flow velocities in x- and y directions, respectively, q is the non-hydrostatic pressure which is normalised by the density, g is gravitational acceleration, $C_f$ is the dimensionless bottom friction coefficient, and $\tau_{xx}, \tau_{xy}, \tau_{yx}$ and $\tau_{yy}$ are the horizontal turbulent stress terms.

The integral of the non-hydrostatic pressure gradient in Eq. 11 can be expressed as (Stelling & Zijlema, 2003):

$$\int_{-d}^{\zeta}\frac{\partial q}{\partial x}dz = \frac{1}{2}h\frac{\partial q_b}{\partial x} + \frac{1}{2}q_b\frac{\partial(\zeta - d)}{\partial x} \tag{13}$$

with $q_b$ the non-hydrostatic pressure at the bottom. Eq. 12 can also be subjected to similar expression. An additional expression is needed to solve for the quantity $q_b$ Stelling & Zijlema (2003) demonstrated that an accurate expression for this can be derived using the Keller-box method:

$$\frac{q|_{z=\zeta} - q|_{z=-d}}{h} = -\frac{q_b}{h} = \frac{1}{2}\frac{\partial q}{\partial z}\bigg|_{z=\zeta} + \frac{1}{2}\frac{\partial q}{\partial z}\bigg|_{z=-d} \tag{14}$$

Further, we introduce $w_s$ and $w_b$ the vertical velocities at surface and bed levels respectively. Note that the non-hydrostatic pressure at the free surface is zero. The momentum equations for these vertical components are

$$\frac{\partial w_s}{\partial t} + \frac{\partial q}{\partial z}\bigg|_{z=\zeta} = 0, \frac{\partial w_b}{\partial t} + \frac{\partial q}{\partial z}\bigg|_{z=-d} = 0 \tag{15}$$

where both the diffusive and advective terms have been neglected as they are generally small compared to the vertical acceleration which is assumed to be instantaneously determined by the non-hydrostatic pressure gradient. Combination of Eqs. 14 and 15 gives

$$\frac{\partial w_s}{\partial t} = \frac{2q_b}{h} - \frac{\partial w_b}{\partial t} \tag{16}$$

The following kinematic condition is used for estimating vertical velocity at the bottom, $w_b$:

$$w_b = -u\frac{\partial d}{\partial x} - v\frac{\partial d}{\partial y} \tag{17}$$

Further, the conservation of local mass yields to

$$\frac{\partial u}{\partial x} + \frac{\partial v}{\partial y} + \frac{w_s - w_b}{h} = 0 \tag{18}$$

Now that we have the required equations, this model can be solved in the original way using a leapfrogging scheme as proposed in Zijlema *et al.* (2011) and Stelling & Zijlema (2003). Alternatively, this problem can be solved as prescribed in Costanza & Carlo (2016) aimed at simulating both non-linear and dispersive shallow water processes using a single layer. Here, the total pressure is decomposed into its hydrostatic and dynamic components to solve a hydrostatic problem and a non-hydrostatic problem sequentially, in the framework of a fractional time step procedure. However, this procedure is complicated as it aims to solve for highly irregular topographies. Yamazaki *et al.* (2009) provides a simple fractional time-step method for the 1-layer SWASH equations involving a hydrostatic time-step followed by a non-hydrostatic time-step. This is the approach implemented in the current project.

### 2.2.3 Equivalence of SWASH with Boussinesq-type equations and Serre-type equations

Assuming a single vertical layer, the SWASH and the Boussinesq-type equations are the same shallow water equations with a non-hydrostatic pressure term. Note that, usually the non-hydrostatic pressure is assumed to have have a linear distribution for both the SWASH and the Boussines-type equations. However, Jeschke *et al.* (2017) has analytically proved that assuming a quadratic pressure distribution will make the models equivalent to Serre-type equations. Further, Wang *et al.* (2020) has developed a 2D model based on the equations by Jeschke *et al.* (2017) and demonstrated the validity through the numerical results. In conclusion, the use of Shallow water equations with non-hydrostatic pressure correction is well justified given that for a single vertical layer the three types of depth averaged Navier-Stokes equations provide similar results.

# 3 Methodology

## 3.1 Modelling approach

A hybrid model is proposed to model coastal flooding. The general shallow water equations can be used to approximately describe these phenomena. However, they are based on hydrostatic pressure balance and the validity of this falls when the waves are small or propagating over varying bathymetry. So, the non-hydrostatic pressure effects are to be considered here.

The evolution of waves near shore is governed by a series of phenomena. First, the waves propagating from deep water experience shoaling as they approach the beach slope. Due to shoaling, the wave height increases and the wavelength decreases when a deep water wave propagates into shallower waters. This results in the steepening of the waves and after a certain depth, the waves become steep enough to break. The computational domain is divided into three zones (see figure 5) and the different equations are used to model each zone so that the important phenomena in that zone are accurately modelled while approximating other phenomena:

**ZONE 1:** Full non-hydrostatic shallow water equations (see section: 3.2)

**ZONE 2:** Non-hydrostatic shallow water equations without the pressure terms

**ZONE 3:** Hydrostatic model(see section: 3.4)

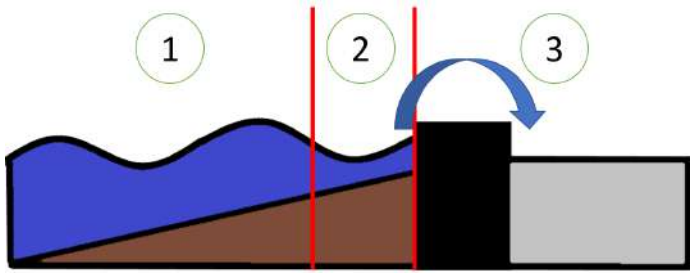


*Figure 5: Modelling approach.*

In zone one, the non-hydrostatic shallow water equations are used to capture the be-

haviour of short waves and shoaling. However, the non-hydrostatic pressure balance can be neglected after the waves break. Since, the vertical resolution of just 1 layer, using hydrostatic pressure from the onset of breaking which ensures that the wave, due to the absence of dispersive effects, quickly transitions into a bore-like shape. Therefore, in zone two the hydrostatic model with advection is considered. This also reduces the Poisson pressure system to be solved in each step.

However, the boundary between zones 1 and 2 must be calibrated to make sure all the waves in the spectrum are breaking before entering zone 2. Further, a set-up correction is to be devised to compensate for the hydrostatic assumption in zone 2. In zone three, it is not required to model any hydrodynamic phenomena since it just has to model the over-topped water from the sea wall. The hydrostatic model for flood propagation by Bates *et al.* (2010) is used here.

In summary, the hybrid model will be derived in this section. The hybrid model will three zones which zone 1 in the offshore boundary, zone 2 which is from the bifurcation depth to the over-topping point, and zone 3 the flood propagation zone. The bifurcation point is derived by parametrizing the breaking depth using the wave saturation approach. A set-up parametrization is attempted as there might be a need for set-up correction.

In zone 1, the non-hydrostatic model from SWASH (Zijlema *et al.*, 2011) is implemented. In zone 2, hydrostatic shallow water equations are implemented which are SWASH equations without the non hydrostatic pressure term. In zone 3, the flooding model based on hydrostatic shallow water equations proposed by Bates *et al.* (2010) is implemented.

## 3.2 Non-Hydrostactic model description

The Non-hydrostatic model uses shallow water equations from SWASH Equations 10, 11, and 12 (see section 2.2.2). The method used here is adapted from Yamazaki

*et al.* (2009). Here, the elevations are solved with the same discretisation as the hydrostatic model(see equation 46). The momentum equations are evaluated in two steps. The first step is estimating velocities without non-hydrostatic pressure. The second step is applying a non-hydrostatic pressure correction to the velocities in step one.

### 3.2.1 Numerical Scheme

The numerical scheme is only derived for 1D momentum equation(Since it is similar for 2D case). Starting from 1-D shallow water equations with Non-Hydrostatic pressure balance.

$$\frac{\partial u}{\partial t} + u\frac{\partial u}{\partial x} = -g\frac{\partial \zeta}{\partial x} - \frac{1}{2}\frac{\partial q_b}{\partial x} - \frac{1}{2}\frac{q_b}{h}\frac{\partial(\zeta - d)}{\partial x} - C_f\frac{u|u|}{h} + \frac{2\nu_t}{h}\left(\frac{\partial}{\partial x}\left(h\frac{\partial u}{\partial x}\right)\right) \quad (19)$$

To reduce complexity of the derived numerical scheme, the equation 19 is discretised as:

$$\frac{\partial u}{\partial t} = -ADV_i - SGrad_i - \frac{1}{2}\frac{\partial q_b}{\partial x} - \frac{1}{2}\frac{q_b}{h}\frac{\partial(\zeta - d)}{\partial x} - FRIC_i + VISC_i \quad (20)$$

Where, advection ($ADV_i$) is discretised using a momentum conserving scheme proposed by Zijlema *et al.* (2011).

$$ADV_i = \frac{1}{h_i^k}\left(\frac{\phi_{i+1}^k\overline{U_{i+1}^k} - \phi_i^k\overline{U_i^k}}{\Delta x}\right) - \frac{U_i^k}{h_i^k}\left(\frac{\phi_{i+1}^k - \phi_i^k}{\Delta x}\right) \quad (21)$$

Where, $\overline{U_i^k}$ is the velocity at cell center and $\phi_i^k$ is the velocity flux at cell center. The surface gradient(SGradi), bottom friction ($FRIC_i$) and viscosity ($VISC_i$) are discretised as:

$$SGrad_i = g\frac{\zeta_i^k - \zeta_{i-1}^k}{\Delta x} \quad (22)$$

$$FRIC_i = C_f\frac{U_i^{k+1}\left|U_i^k\right|}{h_i^k} \quad (23)$$

$$VISC_i = \frac{\nu_i}{h_i^k}\frac{h_i^k\left(U_{i+1}^k - U_i^k\right) - h_{i-1}^k\left(U_i^k - U_{i-1}^k\right)}{\Delta x^2} \quad (24)$$

The eddy Viscosity term is considered as ad hoe with smagorinsky eddy viscosity(Smagorinsky, 1963).

From section 2.2.2, the equations 16, 17, and 18 can be respectively discretised as:

$$w_{s_i}^{n+1} = \frac{2\Delta t q_{b_i}^{k+1}}{h_i^k} - w_{b_i}^{n+1} + w_{b_i}^n + w_{s_i}^n \tag{25}$$

$$w_{b_i}^{n+1} = -\left(\frac{\tilde{U}_i^{k+1} + \left|\tilde{U}_i^{k+1}\right|}{2}\right)\frac{d_i - d_{i-1}}{\Delta x} - \left(\frac{\tilde{U}_i^{k+1} - \left|\tilde{U}_i^{k+1}\right|}{2}\right)\frac{d_{i+1} - d_i}{\Delta x} \tag{26}$$

$$\frac{U_{i+1}^{k+1} - U_i^{k+1}}{\Delta x} + \frac{w_{s_i}^{n+1} - w_{b_i}^{n+1}}{h_i^k} = 0 \tag{27}$$

**STEP 1**

Solve the velocity for hydrostatic time-step. From equation 20 :

$$\hat{U}_i^{k+1} = \frac{U_i^k - \Delta t \times (ADV_i + SGrad_i + VISC_i \times \text{ break }_i)}{1 + C_f \Delta t \frac{U^4}{h_i^4}} \tag{28}$$

Here, break $_i$ is the breaking flag for ad hoe viscosity. Note that for the zone two(see figure 5 ) only step one is carried out.

**STEP 2**

Assume only the dynamic pressure component is retained in the Non-Hydrostatic time-step:

$$U_i^{k+1} = \tilde{U}_i^{k+1} - \frac{\Delta t}{2\Delta x}\left(q_{b_i}^{k+1} - q_{b_{i-1}}^{k+1}\right) - \frac{\Delta t}{2h_i^k}\left(q_{b_i}^{k+1} + q_{b_{i-1}}^{k+1}\right)\left(\frac{\zeta_i^k - \zeta_{i-1}^k - d_i + d_{i-1}}{\Delta x}\right) \tag{29}$$

Equation 29 can be written as

$$U_i^{k+1} = \tilde{U}_i^{k+1} - \frac{\Delta t}{2\Delta x}\left(q_{b_i}^{k+1} - q_{b_{j-1}}^{k+1}\right) - \frac{\Delta t}{2\Delta x}\alpha_i\left(q_{k_i}^{k+1} + q_{b_{i-1}}^{k+1}\right) \tag{30}$$

where,

$$\alpha_i = \frac{\Delta x}{h_i^k}\left(\frac{\zeta_i^k - \zeta_{i-1}^k - d_i + d_{i-1}}{\Delta x}\right)$$

Substituting Equations 25, 30 to 26 will result in tridiagonal pressure system(pentagonal for 2D case )

$$A_{i,j-1}q_{b_{-1}}^{k+1} + A_{i,i}q_{b_i}^{k+1} + A_{i,i+1}q_{b_{+1}}^{k+1} = B_i \tag{31}$$

Where,

$$A_{i,t-1} = \frac{\Delta t}{2\Delta x^2}\left(-1+\alpha_i\right) \tag{32}$$

$$A_{i,i} = \frac{\Delta t}{2\Delta x^2}\left(2+\alpha_i-\alpha_{i+1}\right)+\frac{2\Delta t}{\left(h_i^k\right)^2} \tag{33}$$

$$A_{i,i+1} = \frac{\Delta t}{2\Delta x^2}\left(-1-\alpha_{i+1}\right) \tag{34}$$

$$B_i = -\frac{\tilde{U}_{i+1}^{k+1}-\tilde{U}_i^{k+1}}{\Delta x}-\frac{-2w_{b_i}^{n+1}+w_{b_i}^n+w_{s_i}^n}{h_i^k} \tag{35}$$

This system is solved using Bi-CGSTAB(Bi-Conjugate Gradient Stabilized) method with an ILU pre-conditioner. Pythons inbuilt sparse solver library is used to perform this. Overall algorithm for velocity calculation for each time step:

- Solve the hydrostatic step to get $\tilde{U}^{n+1}$ (Eq: 28 )
- Use $\tilde{U}^{n+1}$ to solve Eq: 26 to get $w_b^{n+1}$
- Use $\tilde{U}^{n+1}$ and $w_b^{n+1}$ to solve the Poisson system (Eq: 31) and get $q_b^{k+1}$
- Use $q_b^{k+1}$ in Eq: 29 to get $U^{k+1}$ and in Eq: 25 to get $w_2^{n+1}$

**Wave generation**

To generate waves without reflections, a weakly reflective condition is utilized at the wave incoming open boundaries (Blayo & Debreu, 2005).

$$u_b = \sqrt{\frac{g}{h_b}}\left(2\zeta_b-\zeta+\bar{\zeta}\right) \tag{36}$$

Where, $\zeta_b$ is the incoming wave elevation, $\zeta$ is the current elevation and $\bar{\zeta}$ is mean elevation of the surface. $u_b$ is the evaluated velocity and $h_b$ is the water depth at the boundary.

**The absence of viscosity terms**

The viscosity of a fluid dissipates momentum on large scale fluid motions while turbulence dissipates momentum at the smaller eddies. This is a classical hypothesis in fluid mechanics. However, in Reynolds averaging of Navier-Stokes equations it is demonstrated that the effect of turbulence can be captured by assuming an eddy viscosity on the mean flow. This can also be seen in the shallow water equations(see section 2.2.1) in the form of the effective viscosity $\nu_h$. However, this model neglects viscous terms which results in the lack of an internal dissipation mechanism. However, internal dissipation is one of the important terms to simulate the coastal process of wave breaking. So, an ad hoc eddy viscosity model is implemented in the model(see appendix A).

### 3.2.2 Validation

Any model which claims to model non-hydrostatic pressure must be able to simulate solitary waves. To validate this, a grid convergence study was conducted using periodic Cnoidal waves. The RMSE error for wave elevation is found using the numerical solution acquired for a resolution of 0.1m. The wave characteristics are an amplitude of 1m, a period of 50 seconds, and a water depth of 10m. The RMSE error is calculated as shown in appendix B. The results of this are presented in figure 6.

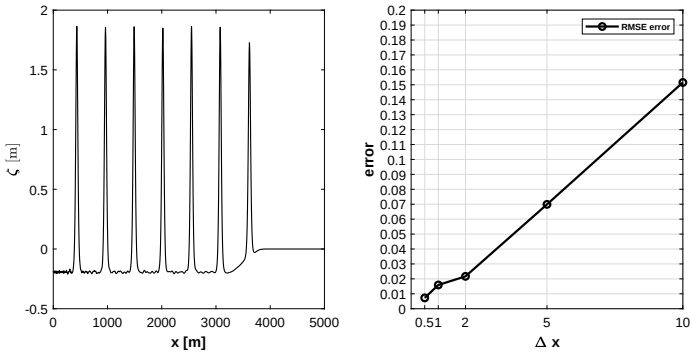


*Figure 6: Grid convergence study with Cnoidal waves.*
*Cnoidal wave elevation for $\Delta x = 0.1$m(left) and error vs grid resolution(right).*

By comparing figures 6 and 12 we can see that the hydrostatic model has acceptable

accuracy for 5m resolution but the non-hydrostatic model requires at least 2m resolution for good results. It should also be noted the Cnoidal waves are quite extreme and therefore 2m is not to be considered as the maximum resolution for accurate results for short waves which occur near shore.

## 3.3 Bifurcation depth derivation and wave set-up correction

The reason for dividing the non-hydrostatic model is based on two factors:

1. The first factor is wave breaking. Since the vertical resolution of the model is just one layer. It is advised to switch off non-hydrostatic pressure after the onset of breaking. This allows the wave to transform into a bore-like shape and simulate effects of breaking.

2. The speed of the model can drastically increased by the reducing the pressure Poisson system to be solved every time-step.

First to find where most waves break, a breaking depth scatter diagram(see figure 7) was made using the saturation approach presented in Battjes (1974)(see appendix A). The scatter digram was made for the ranges of values in table 1.

| | |
|---|---|
| $\boldsymbol{H}_0$[m] | $0.1 - 4$[dH $= 0.1$m] |
| $\boldsymbol{T}_0$[s] | $1 - 30$[dT $= 0.5$s] |
| $\boldsymbol{\beta}$ | $0.05, 0.025, 0.0167, 0.0125,$ and$0.01$ |

*Table 1: Ranges of values considered for breaking depth scatter. Where, $H_0$ is the deep water wave height, $T_0$ is the period and $\beta$ is the beach slope.*

System of equations to solve for breaking depth using saturation approach:

$$H_b = \gamma d_b \tag{37}$$

$$K_s = \frac{H_b}{H_0} = \sqrt{\frac{2\cosh^2(kd_b)}{2kd_b + \sinh(2kd_b)}} \tag{38}$$

$$\omega^2 = gk\tanh(kd_b) \tag{39}$$

Where, $H_b$ and $d_b$ are the breaking height and depth, and $K_s$ is the shoaling coefficient. All equations are obtained from linear potential wave theory(Dean & Dalrymple, 1991).

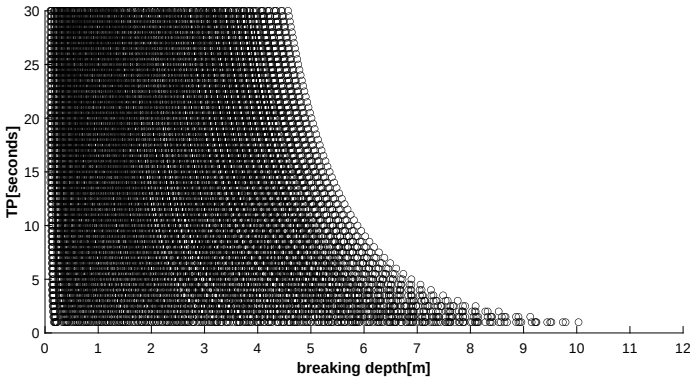


*Figure 7: Breaking depth scatter diagram based on saturation approach*

Since, the calculation of breaking depth through saturation approach requires an iterative solution. It is preferable to make a simple parametric expression for determining the breaking depth. It is also to be noted that the bifurcation depth has be before or at the onset of wave breaking. Two parameters offshore wave height($H_0$) and wave breaker index($\gamma$) where selected to parametrize the breaking depth. After visually analysing the behaviour of breaking depth with changes in individual parameters, the following expression is obtained:

$$d_b = (0.798H_0^2 + 3.514)\exp(-1.459\gamma) \tag{40}$$

The parametric model is compared with the saturation approach in figures 8 and 9. The model fits well, with a coefficient of determination $R^2 = 0.9657$ and a root-mean-square deviation $rms\Delta = 0.2903$ meter.

When compared with time periods(see figure 9), the custom model is found to fit well for short waves(periods of 1-15 seconds) and overestimate for high time periods. This is acceptable as the non-hydrostatic pressure is only to be resolved for short waves and long waves are not highly affected by this.

The custom made model is found to slightly overestimate the breaking depth for mid wave heights and underestimate for very low and very high wave heights(see figure 8). Overall, the custom model is found to be accurate for Irribarren numbers of 0 -

0.3 which is actually the region where wave saturation approach is valid. Note, the saturation approach for wave breaking is only valid for dissipative environments.

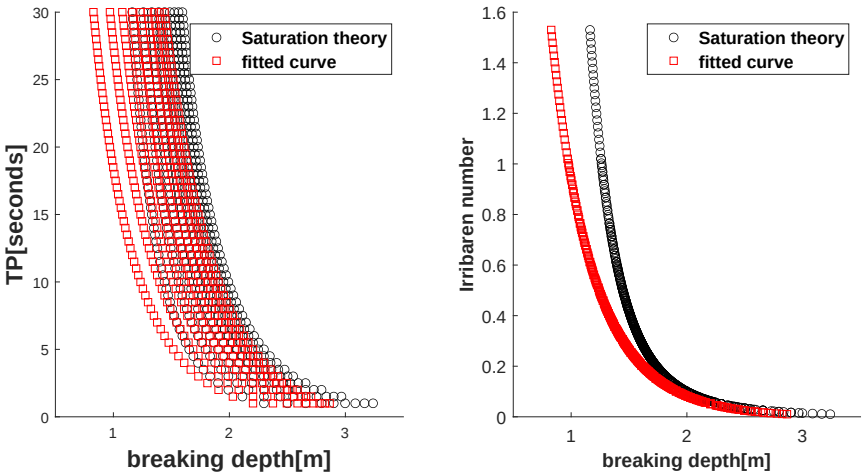


*Figure 8: Breaking depth scatter diagram using custom fit.*
*$H_0$'s of 0.1-4m, time period 15 seconds and beach slopes of $\beta$ = [0.0500,0.0250,0.0167,0.0125,0.0100]*

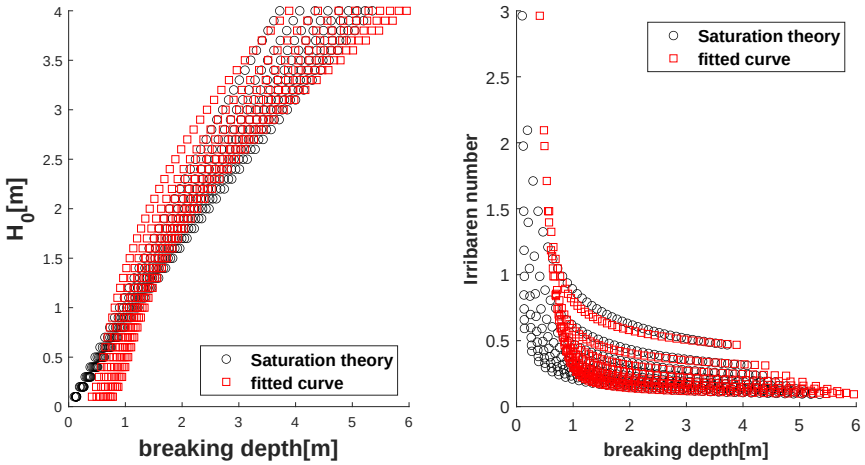


*Figure 9: Breaking depth scatter diagram using custom fit.*
*$H_0$ of 1.5m, time periods 1-30 seconds and beach slopes of $\beta$ = [0.0500,0.0250,0.0167,0.0125,0.0100]*

## Set-up correction

The wave set-up is crucial to wave over-topping and thus to coastal flooding and the hybrid model may result in inaccurate set-up which needs to be corrected. For this, a parametric expression is derived using least squares fitting of set-up obtained from SWASH. As a starting point of this derivation, the formulation provided by Stockdon *et al.* (2006) is used:

$$< \eta >= 0.35\beta_f \sqrt{H_0 L_0} \tag{41}$$

Where, $H_0$ and $L_0$ are deep water wave height and wave length. $\beta_f$ is the surf-zone slope. Stockdon *et al.* (2006) states that the model has a coefficient of determination $R^2 = 0.48$ and a root-mean-square deviation $rms\Delta = 0.213$ meter.

Since this is highly inaccurate, a parametric model $< \eta >= a\beta_f^b \sqrt{H_0 L_0}$ is fitted using MATLAB using least square approach. The coefficients a and b were found to be 0.1874 and 0.5948 respectively. Furthermore, the model fits with a coefficient of determination $R^2 = 0.8805$ and a root-mean-square deviation $rms\Delta = 0.0889$ meter.

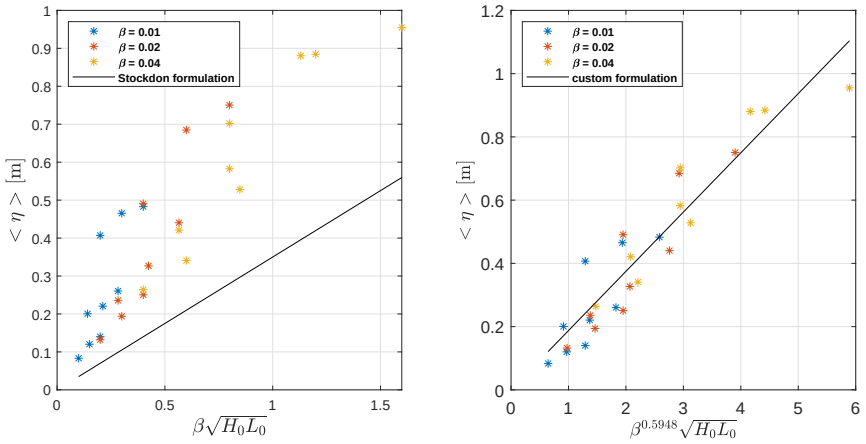


*Figure 10: Set-up correction comparison with SWASH. The discrete values are obtained from SWASH and the fitting line is as mentioned in the respective legend.*

The stockdon model and the custom model were compared with set-up values obtained from the SWASH model in figure 10. SWASH simulations are made for the ranges of the values in table 2.

| | |
|---|---|
| $\boldsymbol{H}_0$[m] | $1, 2,$ and$4$ |
| $\boldsymbol{T}_0$[s] | $8, 12,$ and$16$ |
| $\boldsymbol{\beta}$ | $0.01, 0.02,$ and$0.04$ |

*Table 2: Ranges of values considered for parametric wave set-up definition.*
*Where, $H_0$ is the deep water wave height, $T_0$ is the period and $\beta$ is the beach slope.*

The custom fitted set-up equation is:

$$< \eta >= 0.1874 \beta_f^{0.5948} \sqrt{H_0 L_0} \tag{42}$$

It should be noted that a parametric model for wave set-up with the current available parameters is not feasible due to the slightly poor fit of the model. Fortunately, it is found in section 4.2 that the set-up need not be corrected for the hybrid model.

## 3.4 Hydrostactic model description

The current model is primarily based on the work of Bates *et al.* (2010) where a set of equations are derived from the shallow-water equations. The model uses 2D raster cells for water level elevation. Although, it was first proposed in Bates & De Roo (2000), the improved version from Bates *et al.* (2010) is implemented here. Bates *et al.* (2010) uses velocity fluxes instead of velocities and it is found the when the non-hydrostatic pressure is implemented in the form of fluxes, it causes severe underestimation of water levels. So, the equations from (Bates *et al.*, 2010) are used as velocity equations instead of fluxes. The governing partial differential equations for mass and momentum conservation are given as:

$$\frac{\partial \zeta}{\partial t} + \frac{\partial hu}{\partial x} + \frac{\partial hv}{\partial y} = 0 \tag{43}$$

$$\frac{\partial u}{\partial t} + g\frac{\partial \zeta}{\partial x} + \frac{C_f u|u|}{h} = 0 \tag{44}$$

$$\frac{\partial v}{\partial t} + g\frac{\partial \zeta}{\partial y} + \frac{C_f v|v|}{h} = 0 \tag{45}$$

where $\zeta$ is the free-surface elevation [m] w.r.t. the reference level $z = 0$ and h is the water depth [m] defined as $\mathrm{h} = \zeta + \mathrm{d}$( see figure 11), $u$ and $v$ are the depth averaged velocities in $x$ - and $y$ -direction $[m^2/s]$, $C_f$ is the Manning friction coefficient and g the gravitational acceleration $[m/s^2]$. Equations 44 and 45 are derived from the 1D shallow-water momentum equations (see section 2.2.1) by neglecting the advection terms.

### 3.4.1 Numerical Scheme

The scheme uses a staggered Cartesian rectilinear grid. The surface elevation ($\zeta$) and the bottom depth(d) are defined in the center of the cell. The flow depth(h), flow velocities(U,V) and the fluxes are defined at cell edges, see figure 11. This requires the interpolation of flow depths using the elevation and bottom depth from the cell centres.

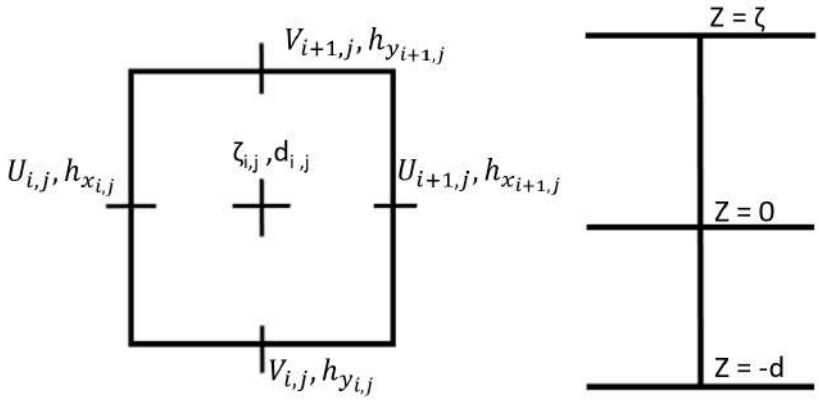


*Figure 11: Staggered computational grid used for the model(Left). Definition of bottom depth(d), mean water level and surface elevation($\zeta$)(Right).*

The continuity equation is discretized using first order backward finite difference for the spatial derivatives and a first order forward finite difference for time derivatives:

$$\zeta_{i,j}^{k+1} = \zeta_{i,j}^{k} - \Delta t \left[ \frac{u_{i+1,j} h_{x_{i+1,j}} - u_{x_{i,j}} h_{x_{i,j}}}{\Delta x} + \frac{v_{i,j+1} h_{y_{i,j+1}} - v_{i,j} h_{y_{i,j}}}{\Delta y} \right] \tag{46}$$

Where, $i = 1, \ldots . M$ and $j = 1, \ldots N$ are the Cartesian grid indexes. This scheme needs the Courant-Friedrichs-Lewy (CFL) stability condition(Courant *et al.*, 1928) for stability in time. It is further discussed in section 3.4.1.

The momentum equations are discretized as described in Van Engelen (2016) which is slightly different from (Bates *et al.*, 2010). The method used is the same explicit first order finite difference method used by (Bates *et al.*, 2010). However, the velocities

$(u, v)$ are calculated as a weighted average of the velocity in previous time-step and the average velocity in neighbouring cells in the previous time-step. See weighted expressions A and B in equations 47 and 48:

$$u_{i,j}^{k+1} = \frac{\overbrace{\theta.u_{i,j}^{k} + (1-\theta).\frac{u_{i+1,j}^{k} + u_{i-1,j}^{k}}{2}}^{A} - g.\Delta t.\frac{\zeta_{i,j}^{k} - \zeta_{i-1,j}^{k}}{\Delta x}}{1 + \Delta t.\left[\frac{C_{f_{i,j}}|u_{i,j}^{k}|}{h_{x_{i,j}}^{k}}\right]} \tag{47}$$

$$v_{i,j}^{k+1} = \frac{\overbrace{\theta.v_{i,j}^{k} + (1-\theta).\frac{v_{i,j+1}^{k} + v_{i,j-1}^{k}}{2}}^{B} - g.\Delta t.\frac{\zeta_{i,j}^{k} - \zeta_{i,j-1}^{k}}{\Delta y}}{1 + \Delta t.\left[\frac{C_{f_{i,j}}|v_{i,j}^{k}|}{h_{y_{i,j}}^{k}}\right]} \tag{48}$$

Van Engelen (2016) found that this spatial averaging will limit the instabilities and result in a smoother solution. Higher values of $\theta$ produce smoother solutions due to local numerical diffusion at the expense of accuracy. The value of the weighting factor $\theta$ must be close to 1 to reduce inaccuracies in the results.

## Stability condition

The CFL(Courant *et al.*, 1928) number is a necessary stability criteria for any explicit time-step scheme to converge to a hyperbolic partial differential equation. Given, the discretization in time as $\Delta t$ and in space as $\Delta x$ and the characteristic velocity of the system as $U$. The CFL number must be ensured to be less than 1 to ensure stability.

$$CFL = \frac{U\Delta t}{\Delta x} < 1 \tag{49}$$

Using the approximation of shallow water wave celerity for the characteristic velocity we get:

$$\Delta t < \frac{\Delta x}{\sqrt{g h_t}} \tag{50}$$

Where, $h_t$ is the maximum water depth in the time-step. However,it was found that the condition in Eq:50 alone was not enough to ensure stability and Bates

*et al.* (2010) proposed a relaxation factor $\alpha$ to ensure stability and validated it with multiple floodplain simulations.

$$\Delta t < \alpha \frac{\Delta x}{\sqrt{g h_t}}, \qquad \alpha = 0.2 - 0.7 \tag{51}$$

### 3.4.2 Model limitations

**Neglecting advection terms**

The current model based on Bates *et al.* (2010), neglects advective terms. The justification for this is that the advective transport of momentum is negligible for short waves and the near shore region is dominated by longer infragravity waves. Further, Hunter *et al.* (2007) justified this by scaling the continuity and momentum equations based on dimensional analysis of the shallow water equations. Van Engelen (2016) conducted a dimensional analysis of the shallow water equations in appendix A using the dimensional quantities prescribed by Hunter *et al.* (2007) and found that it is reasonable to assume that for infragravity waves with a moderate height of 0.25 - 1 meter and period in the range of 33 - 500 seconds, propagating in the nearshore region, the advection term plays only a minor role and can be neglected.

**Dependence on bottom friction**

The inertial formulation of the model is found to be highly unstable for low manning roughness values(n $\sim$ 0.01) and this is also observed by Bates *et al.* (2010). It is evident that the bottom friction acts as numerical stability mechanism and model cannot function when there are areas with low friction. So, care should be taken when using this model for domains where large areas of low friction lands dominate.

### 3.4.3 Validation

A grid convergence study was conducted for a standing wave in a half closed basin with the length of one wavelength. The bottom is considered friction less by assigning a negligible friction coefficient. The incoming wave has an amplitude of 1 meter and a period of 26 seconds. The water-depth was set at 10 meters (see Figure 12).

To understand the effect of grid resolution, two types errors with respect to the

analytical solution of the standing wave were estimated. The first error is the RMSE(Root Mean Square Error) error of the wave elevation:

$$RMSE = \sqrt{\frac{1}{N}\sum[\zeta - \zeta_{analytical}]^2} \tag{52}$$

The second error is the volume error:

$$volume \;\; error = |1 - \frac{V}{V_{analytical}}| \tag{53}$$

For definition of error definitions and analytical solution of the standing wave see appendix B.

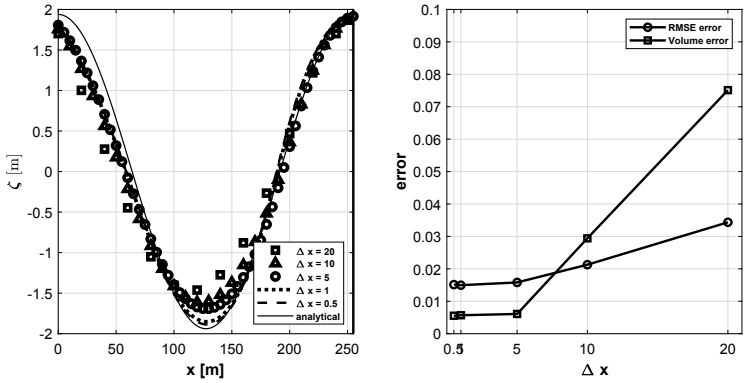


*Figure 12: Grid convergence study with H = 4m, T = 26s, h = 10m and n = 0.0001. wave elevation(left) and error vs grid resolution(right).*

Five grid resolutions $\Delta x = 0.5$, 1, 5, 10 and 20m were considered for the study. It is observed that, there is no significant reduction in the RMSE and volume errors below a resolution of 5m. Also, the increase in volume error is higher than the increase in RMSE error for resolutions greater than 5m(see figure 12).

To verify two dimensional wave propagation, a radially symmetric Gaussian wave is initiated at the centre of the domain. The domain is of the dimensions 1000×1000 meter with open boundaries on all four sides. The two dimensional initial Gaussian elevation adapted is from Aydin (2011). It is defined as:

$$\zeta_0(x,t) = a\exp(-\frac{(x-x_0)^2}{2\sigma_x^2} - \frac{(y-y_0)^2}{2\sigma_y^2}) \tag{54}$$

where a is the amplitude, $x_0$ and $y_0$ are the center coordinates and $\sigma_x$ and $\sigma_y$ are the spreads in x- and y-direction which were set at 0.15 times the width of the domain.

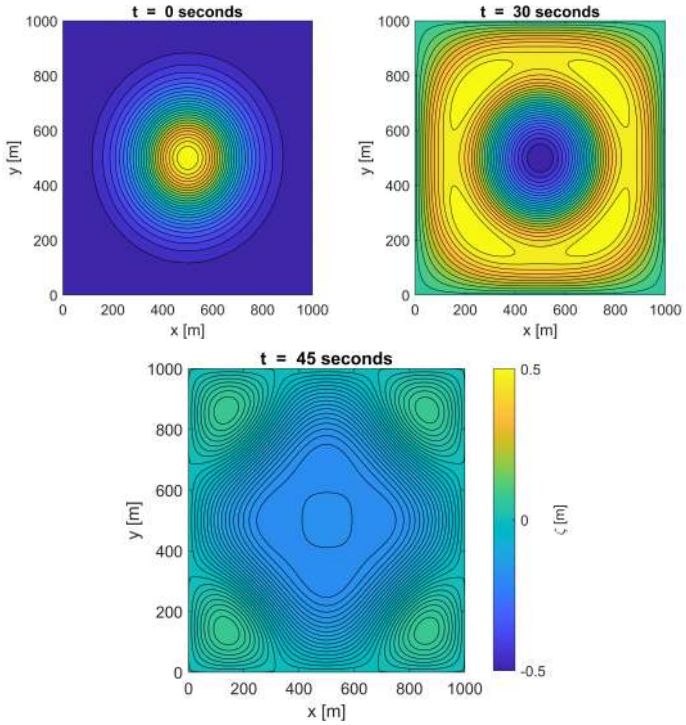


*Figure 13: uniform 2D grid $\Delta x = 5$m, $\Delta y = 5$m, $a_0 = 1$m, $h = 10$m and $n = 0.02$.*

Two simulations were performed, one with a uniform grid $\Delta x = 5$m, $\Delta y = 5$m (see figure 13) and the second with a non-uniform grid $\Delta x = 5$m and $\Delta y = 20$m (see figure 14). It is verified that the two dimensional wave propagation is accurate.

However, as Van Engelen (2016) observed, there is a small degree of artificial reflection due to open boundaries in this method and it is found to be originate at corners. The reason for this is the fact that the open boundary conditions used are derived for a frictionless one-dimensional case with normally incident waves. No studies were conducted for this reflection in Van Engelen (2016) and no further study will be conducted in this research too, as the time frame and scope of the research are limited.

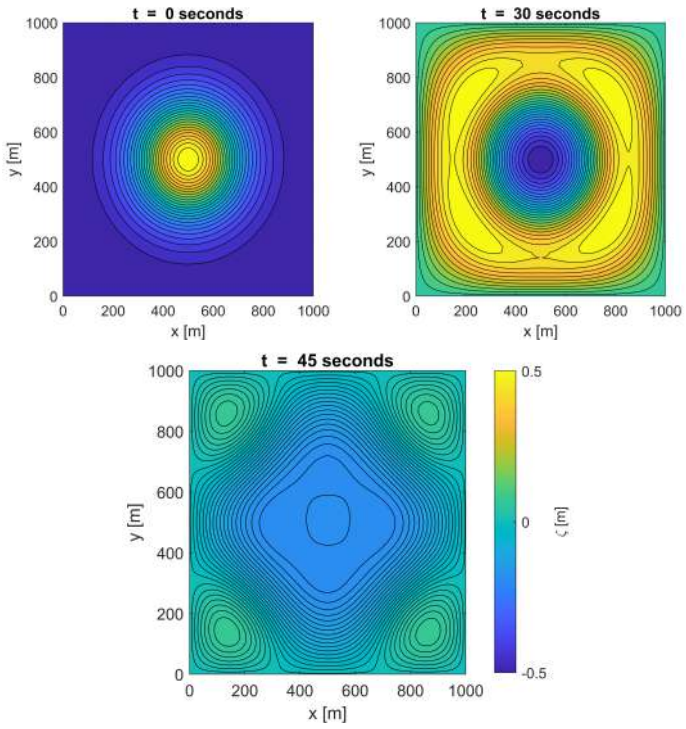


*Figure 14: non-uniform 2D grid $\Delta x$ = 5m, $\Delta y$ = 20m, $a_0$ = 1m, h = 10m and n = 0.02.*

## 3.5 Flooding and drying conditions

The numerical simulation of coastal flood inundation requires a moving waterline which, unlike conventional CFD simulations would require the grid points to switch between wet and dry states. Initially, the wet state is assigned to the cells which have flow depth over a user-specified depth threshold( $h_{threshold}$). The reason for this is to avoid the division by zero error caused in the momentum discretization. A value of 0.0005m is suggested for $h_{threshold}$.

The flooding condition is based on the fact that in a numerical simulation, only one cell can be flooded in the direction of flow in a single time-step. The flooding condition in this model is based on Yamazaki *et al.* (2009). If the flow is positive $x$ direction, $CELL^k_{i,j-1}$ is wet and $CELL^k_{i,j}$ is dry:

$$CELL^{k+1}_{i,j} = \begin{cases} wet, & \text{if} \quad \zeta^k_{i-1,j} - d_{i-1,j} \geq h_{threshold} \\ dry, & \text{if} \quad \zeta^k_{i-1,j} - d_{i-1,j} < h_{threshold} \end{cases}$$

This means the cell is set as wet for computation in the next iteration only if the flow depth of the cell computed using the wave elevation of the previous wet cell is larger

than the threshold value. However, in the current model, an additional condition is set for which the velocity in the previous wet cell must be positive(towards the dry cell) to ensure the cells are only flooded by an advancing flow.

$$CELL_{i,j}^{k+1} = \begin{cases} wet, & \text{if} \quad \zeta_{i-1,j}^{k} - d_{i-1,j} \geq h_{threshold} \quad \&\& \quad u_{i-1,j} > 0 \\ dry, & \text{if} \quad \zeta_{i-1,j}^{k} - d_{i-1,j} < h_{threshold} \end{cases}$$

Additionally, if the cell becomes wet the scheme assigns the flow depth and flux component of the new wet cell as:

$$h_{i,j}^{k+1} = \zeta_{i,j}^{k} + d_{i,j}; \qquad u_{i,j}^{k+1} = u_{i-,j}^{k}$$

The same process is done for the y direction to complete the wet-dry status, if flooding occurs from multiple directions the flow depth is averaged.

The drying conditions are adapted from the Delft3D manual (Deltares, 2014). Although the flooding is done in a cell when the water depth crosses the depth threshold, drying is only done when the water height falls below half of the threshold value. This form of hysteresis is introduced in the flooding-drying conditions to avoid the flip-flop of the cells due to the algorithm. Flip-flop is the switching of the cell to wet and then dry or vice versa in two consecutive time-steps. When the cell is selected to be dried, it's water flow height is set to zero and the surface elevation is set as the water depth and velocities are set as zero.

In this model, three options have been provided for calculating the water depth. They are as follows:

$$h_{x_{i,j}} = \begin{cases} \text{if } OPT == MEAN & \frac{\zeta_{i,j}+\zeta_{i-1,j}}{2} - \frac{d_{i,j}+d_{i-1,j}}{2} \\ \text{if } OPT == MAX & \max\left(\zeta_{i,j}, \zeta_{i-1,j}\right) - \max\left(d_{i,j}, d_{i-1,j}\right) \\ \text{if } OPT == UPWIND & \zeta_{i-1,j} - d_{i-1,j}, \quad \text{if } u_{i,j} > 0 \\ & \zeta_{i,j} - d_{i,j}, \quad \text{if } u_{i,j} < 0 \\ & \max\left(\zeta_{i,j}, \zeta_{i-1,j}\right) - \max\left(d_{i,j}, d_{i-1,j}\right) \quad \text{if } u_{i,j} = 0 \end{cases}$$

The drying and flooding algorithms induce small oscillations in the flow due to their discontinuous nature. This can be reduced by selecting small grid sizes and ensuring bottom gradients are smooth.

# 4 Results and Discussion

In this section, the full non-hydrostatic model is compared with the SWASH model and the level of agreement between the two models is assessed. Then, the hybrid model without any set-up corrections is compared with the full non-hydrostatic model to verify if a set-up correction is necessary based on the level of agreement between them. It is found that the set-up correction is not required for the devised hybrid model. Furthermore, wave over-topping simulations using the hybrid model are compared with the SWASH simulations. A dike shown in figure 23 is used for the over-topping simulations. Finally, simulations of a basic bar profile are compared with SWASH simulations with different bifurcation points.

## 4.1 Comparison of full non-hydrostatic model with SWASH model

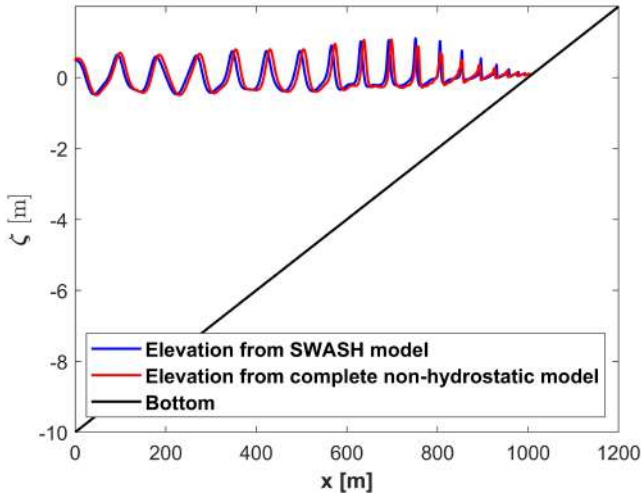


*Figure 15: Comparison of non-hydrostatic model with SWASH $H = 1m$, $T = 10s$, $\beta = 0.01$(slope), $\Delta x = 0.2m$ and $Cf = 0.019$.*

The full non-hydrostatic model is where there is no strict bifurcation of zones 1 and 2 but the non-hydrostatic pressure is still switched off from the onset of wave breaking. This can be seen as having a time varying bifurcation of Zones 1 and 2 due to the moving of the wave breaking location. The moving breakpoint(which is the bifurcation point for full non-hydrostatic model), coupled with the wave height

dictates the accuracy of the results.

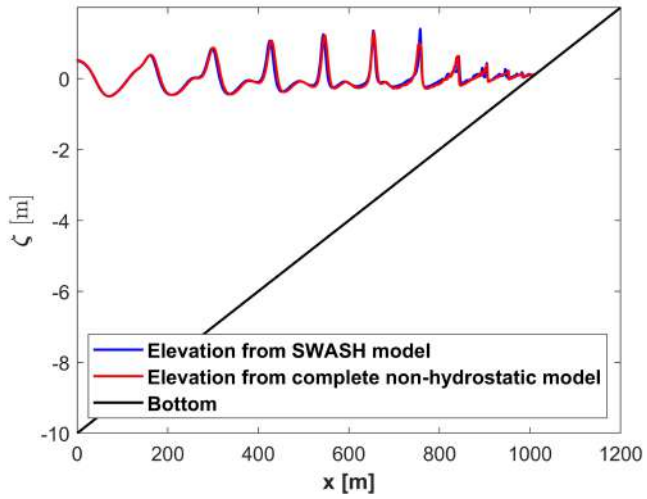


*Figure 16: Comparison of non-hydrostatic model with SWASH $H = 1m$, $T = 16s$, $\beta = 0.01$(slope), $\Delta x = 0.2m$ and $Cf = 0.019$.*

Looking at figures 15, 16, and 17, one may assume that the full non-hydrostatic model agrees with the SWASH results. However, closer examination reveals that the simulations are for a low wave height of 1m. The figure 18, presents the comparison for a large wave height of 4m and one can clearly see the clear disagreement between the two models. This is due to the breaking point being much further offshore which translates into smaller Zone 1 of the domain. Since, non-hydrostatic pressure is only resolved in a small region, the results are highly inaccurate.

It should also be noted that there is additional numerical dissipation in the model compared to SWASH, especially after the bifurcation of the domains. The reason for this is the implementation of different breaking criteria and eddy viscosity models. Although, this leads to lower wave elevations in surf zone, the swash zone and set-up agree very well when compared to SWASH as seen in figures 15, 16, 17, and 18.

The results of full non-hydrostatic model simulations are presented in table 3. The RMSE errors of the elevation, maximum wave set-up from simulations and maximum wave set-up from the derived parametric model were presented for each case.

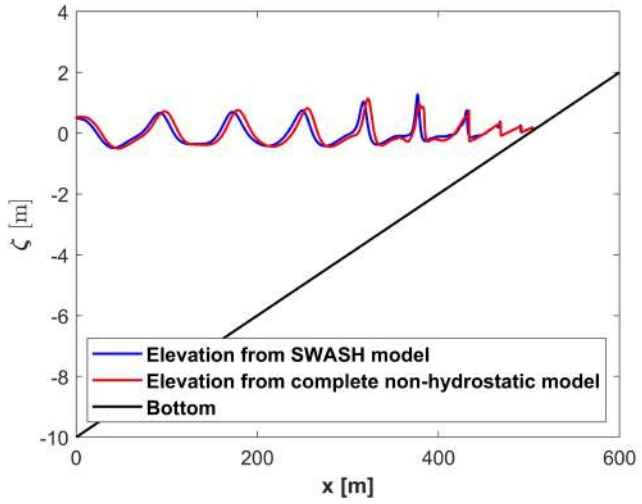


*Figure 17: Comparison of non-hydrostatic model with SWASH H = 2m, T = 10s, $\beta$ = 0.01(slope), $\Delta x$ = 0.2m and Cf = 0.019.*

The RMSE errors of the surface elevation follows the reasoning provided above leading to larger values for higher wave heights. The wave set-up given by the parametric formulation disagrees with the obtained values. However, the model has only a coefficient of determination $R^2 = 0.8805$ and a root-mean-square deviation $rms\Delta = 0.0889$ meter. From figure 10, it can be seen the model does not fit even with SWASH simulations accurately.

| **H**[m] | **T**[s] | $\boldsymbol{\beta}$ | **RMSE**[m] | **setup**[m] | **parametric setup** [m] |
|---|---|---|---|---|---|
| 1 | 8 | 0.01 | 0.1034 | 0.088 | 0.1210 |
| 1 | 10 | 0.01 | 0.0755 | 0.09 | 0.1513 |
| 1 | 12 | 0.01 | 0.1114 | 0.092 | 0.1815 |
| 1 | 16 | 0.01 | 0.1060 | 0.1066 | 0.2420 |
| 2 | 10 | 0.01 | 0.1211 | 0.2105 | 0.2139 |
| 4 | 10 | 0.01 | 0.6260 | 0.5076 | 0.3025 |
| 1 | 10 | 0.02 | 0.0663 | 0.164 | 0.2284 |
| 2 | 10 | 0.02 | 0.1242 | 0.2881 | 0.3231 |

*Table 3: Results of full non-hydrostatic model simulations.*

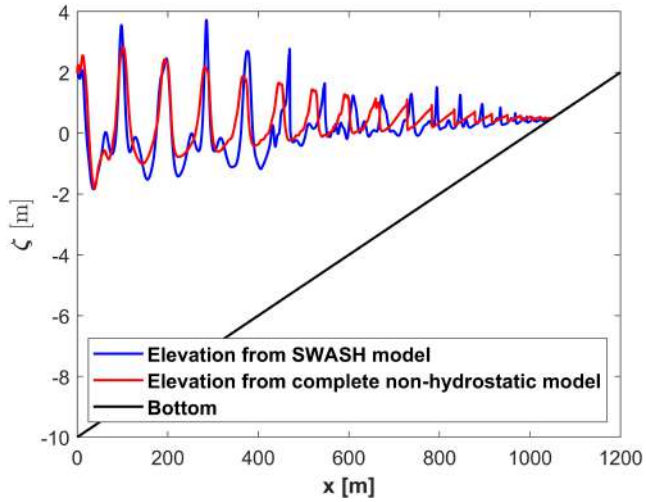


*Figure 18: Comparison of non-hydrostatic model with SWASH $H = 4m$, $T = 10s$, $\beta = 0.01$(slope), $\Delta x = 0.2m$ and $Cf = 0.019$.*

## 4.2 Comparison of the hybrid model with full non-hydrostatic model without set-up correction

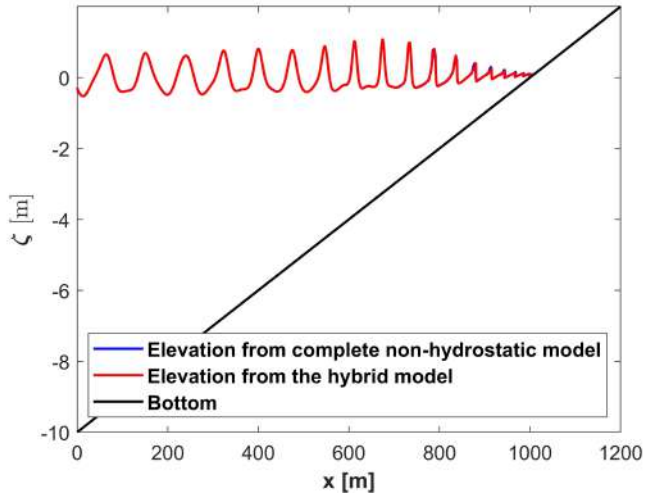


*Figure 19: Comparison of the hybrid model with the full non-hydrostatic model $H = 1m$, $T = 10s$, $\beta = 0.01$(slope), $\Delta x = 0.2m$ and $Cf = 0.019$.*

In this section the hybrid model with a fixed bifurcation depth defined by the parametric breaking point derived in equation 40 is simulated for the same parameters as the full non-hydrostatic model in section 4.1. The results are then compared with the full non-hydrostatic model.

From figures 19, 20, 21, and 22. the parametric set-up correction derived earlier does not seem to be required even for the 4m wave height, since the error from the parametric model is higher than the loss of set-up observed and further, the set-up remains very accurate for the smaller wave heights.

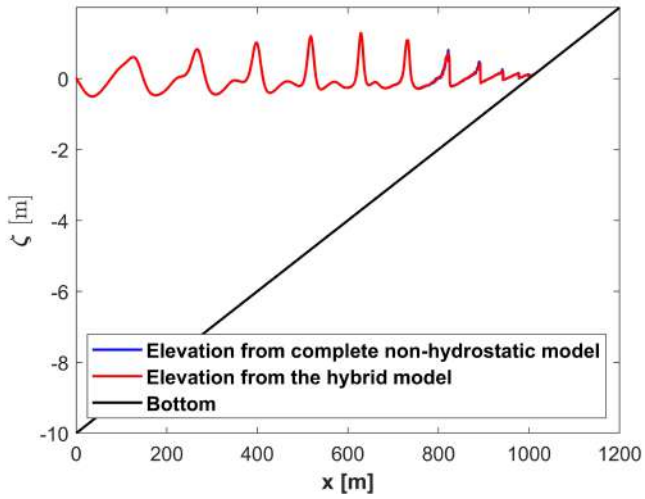


*Figure 20: Comparison of the hybrid model with the full non-hydrostatic model H = 1m, T = 16s, $\beta$ = 0.01(slope), $\Delta x$ = 0.2m and Cf = 0.019.*

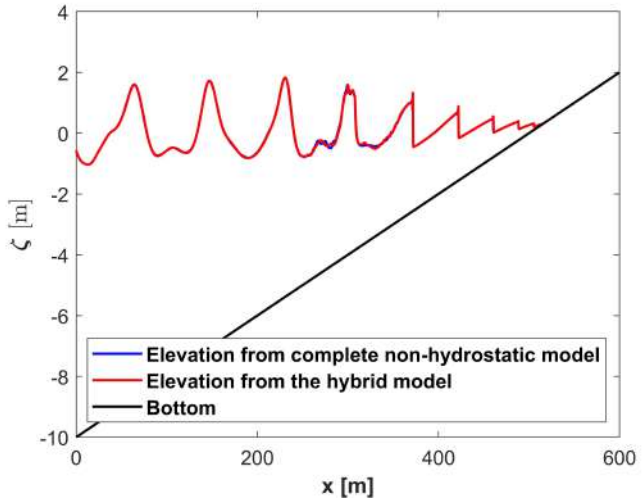


*Figure 21: Comparison of the hybrid model with the full non-hydrostatic model H = 2m, T = 10s, $\beta$ = 0.01(slope), $\Delta x$ = 0.2m and Cf = 0.019.*

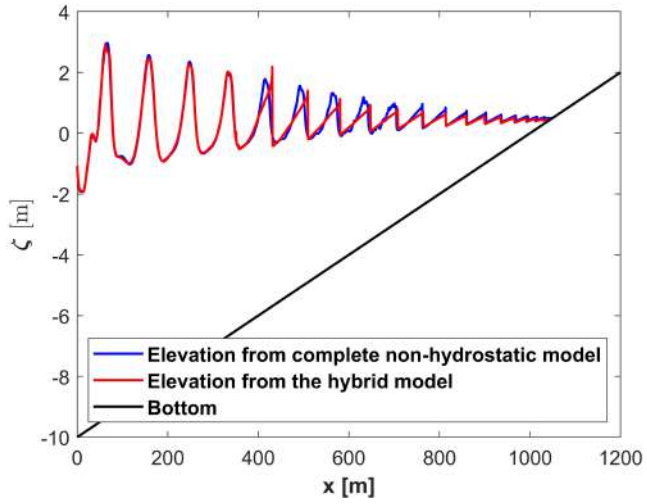


*Figure 22: Comparison of the hybrid model with the full non-hydrostatic model H = 4m, T = 10s, $\beta$ = 0.01(slope), $\Delta x$ = 0.2m and Cf = 0.019.*

| **H**[m] | **T**[s] | $\beta$ | **RMSE**[m] | **Bifurcation depth**[m] |
|---|---|---|---|---|
| 1 | 8 | 0.01 | 0.1034 | 0.088 |
| 1 | 10 | 0.01 | 0.0755 | 0.09 |
| 1 | 12 | 0.01 | 0.1114 | 0.092 |
| 1 | 16 | 0.01 | 0.1060 | 0.1066 |
| 2 | 10 | 0.01 | 0.1211 | 0.2105 |
| 4 | 10 | 0.01 | 0.6260 | 0.5076 |
| 1 | 10 | 0.02 | 0.0663 | 0.164 |
| 2 | 10 | 0.02 | 0.1242 | 0.2881 |

*Table 4: Results of hybrid model simulations without set-up corrections.*

From the table 4, the results of the hybrid model are very close the full non-hydrostatic model even though the later model had time moving bifurcation unlike the hybrid model which has stationary bifurcation point. Although, there is a clear disagreement between the model for the 4m wave height, it is very negligible.

## 4.3 Wave over-topping

The wave over-topping characteristics of the hybrid model are compared for different arrangements of dikes as shown in figure 23. The crest width is kept constant at

5m. The crest height is defined as the height of the crest from mean water level and denoted by $R_c$. Two values of 0.1, and 0.2m are chosen for $R_c$ for the over-topping simulations. The in-slope $\beta$ and out-slope $\beta_{out}$ are set as 0.01.

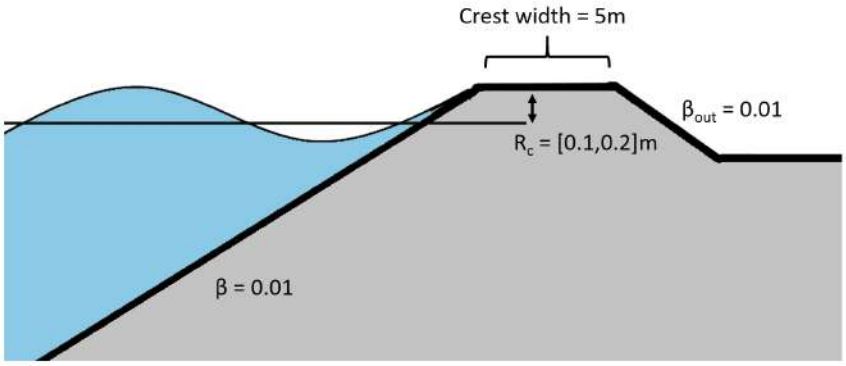


*Figure 23: Representative image for the dikes used in wave over-topping simulations*

The wave over-topping simulations are run for the wave and beach characteristics presented in table 5. The simulations are run for 800 seconds and the first 400 seconds of all simulations are neglected to avoid spin-up effects. Simply put, the spin up time is the time taken by the model to reach a state of statistical equilibrium under the applied forcing. Here, the model must get balanced between the mass and velocity fields in the initial period of time integration.

$$Q(x,t) = U(x,t) \times h(x,t) \tag{55}$$

$$\overline{Q} = \frac{\int_{t_1}^{t_2} Q dt}{t_2 - t_1} \tag{56}$$

The volume flux is defined as shown in equation 55 where, $U$ is the velocity and $h$ water level at that point. The mean volume flux with respect to time is computed between 400 and 800 seconds using the expression in equation 56.

Suzuki *et al.* (2017) conducted a series of 124 over-topping experiments on dikes and compared the experimental results with SWASH simulations. The SWASH simulations are found to reproduce wave characteristics with a low error of 5%. However, at

low discharges SWASH is found to perform very poorly since low discharges are governed by the surface tension(Not modelled in SWASH) and the bottom friction near shore which is poorly modelled in SWASH. Further, Suzuki *et al.* (2017) concluded that the a single layer SWASH model must be accompanied with semi-empirical equations to estimate wave over-topping in an efficient and robust manner.

| Characteristics | | | | SWASH | | Hybrid model | |
|---|---|---|---|---|---|---|---|
| **H**[m] | **T**[**s**] | $\boldsymbol{\beta}$ | $\boldsymbol{R_c}$ [m] | $\boldsymbol{Q_{max}}$ $[\frac{m^3/s}{m}]$ | $\overline{\boldsymbol{Q}}$ $[\frac{m^3/s}{m}]$ | $\boldsymbol{Q_{max}}$ $[\frac{m^3/s}{m}]$ | $\overline{\boldsymbol{Q}}$ $[\frac{m^3/s}{m}]$ |
| 1 | 8 | 0.01 | 0.1 | 0.000042 | 8.2725e-06 | 2.0949e-05 | 1.1123e-06 |
| 1 | 16 | 0.01 | 0.1 | 0.005559 | 0.001086 | 2.0675e-05 | 1.0683e-06 |
| 2 | 8 | 0.01 | 0.1 | 0.1034 | 0.02286 | 0.0223 | 0.0113 |
| 2 | 16 | 0.01 | 0.1 | 0.1388 | 0.04921 | 0.0337 | 0.0118 |
| 3 | 8 | 0.01 | 0.1 | 0.1669 | 0.0837 | 0.0847 | 0.0472 |
| 3 | 16 | 0.01 | 0.1 | 0.3240 | 0.1127 | 0.1280 | 0.0513 |
| 2 | 8 | 0.01 | 0.2 | 0.0280 | 0.0017 | 0.0139 | 0.0048 |
| 2 | 16 | 0.01 | 0.2 | 0.0318 | 0.0073 | 0.0293 | 0.0105 |
| 3 | 8 | 0.01 | 0.2 | 0.0767 | 0.0286 | 0.0493 | 0.0159 |
| 3 | 16 | 0.01 | 0.2 | 0.1751 | 0.0559 | 0.1073 | 0.0353 |

*Table 5: Results of wave over-topping simulations.*

Observing the wave over-topping simulation results from table 5, the hybrid model is found to produce about half the mean and maximum discharges given by SWASH. This, is due to additional dissipation observed in the hybrid model after the bifurcation point as seen in section 4.1. However, as it was suggested by Suzuki *et al.* (2017) for SWASH, the hybrid model must also be accompanied by semi-empirical equations to provide accurate over-topping results. Furthermore, the additional dissipation observed in the hybrid can be corrected in such formulation.

## 4.4 Bar profile with different bifurcation points

A bar profile with all slopes of 0.01 is selected to assess the validity of the model for irregular bottom profiles. The two critical criteria for the bar profiles are wave

breaking and selection of the bifurcation point. The wave breaking condition is not altered in this study as it depends on the local slope. However, the bifurcation point is estimated using the derived parametric expression in equation 40. Here, the average beach slope magnitude is used and the bifurcation depth is found to be 3.42m. Three different bifurcation points can be identified using this depth for the bar profile.

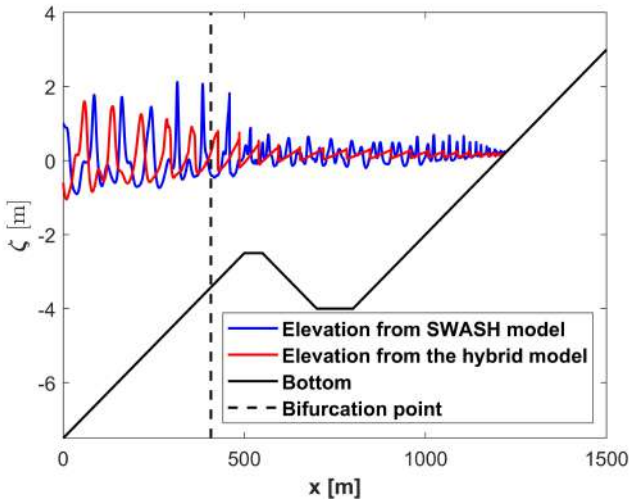


*Figure 24: Comparison of the hybrid model with the SWASH model at the original bifurcation point.*

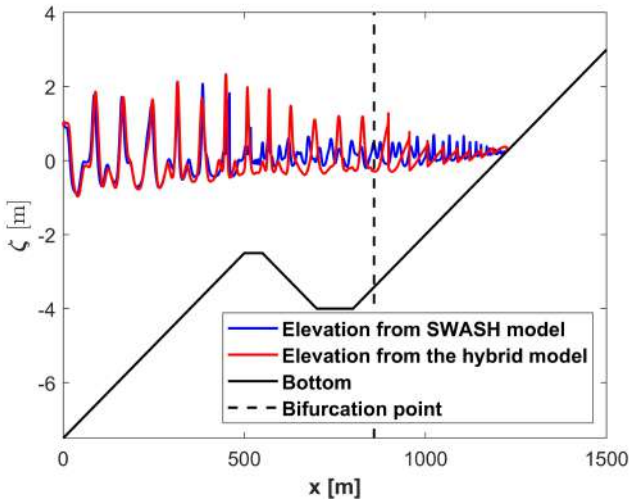


*Figure 25: Comparison of the hybrid model with the SWASH model at an alternate bifurcation point.*

The hybrid model is programmed to bifurcate the domain as shown in figure 24 which as can be seen does not provide accurate results. This might be due to the non-hydrostatic region being highly limited. Further, the hybrid model is made to

bifurcate the zones 1 and 2 at the other two points which are at the same parametric depth as shown in figures 25, and 26. These simulations produced better results in the offshore region of the bar but still fail to produce acceptable results in the depression between the bar and shore. The observations confirm that a bifurcation point closer to the shore provides more accurate results. However, this might not be the case for other irregular topographies and might even be the opposite in some cases.

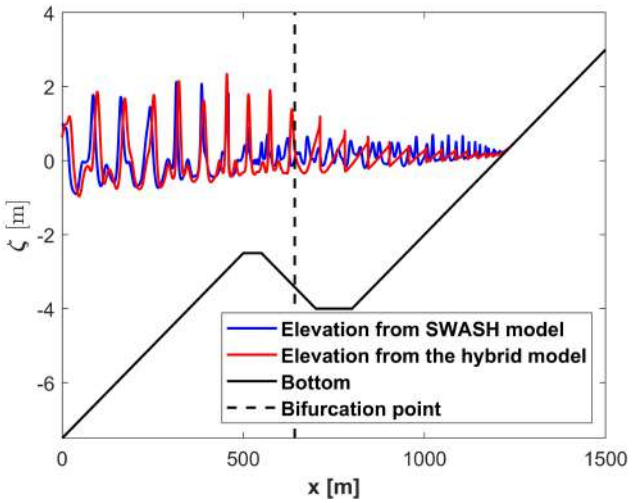


*Figure 26: Comparison of the hybrid model with the SWASH model at an alternate bifurcation point.*

Furthermore, observing figures 24, 25, and 26, it is evident that the waves break just before the bar in both the models. However, the broken waves in SWASH exhibit a slightly non-linear behaviour while propagating from the bar to the next positive(upward) slope. The hybrid model does not model this non-linear behaviour. Further, the SWASH simulations are also run in 1 vertical layer mode which questions the accuracy of SWASH results.

To understand the effect of vertical layers in this scenario, in figure 27 the SWASH model is compared for 1 and 3 layers. The 3-layer SWASH model exhibits higher dissipation at the bar and slightly less non-linear behaviour. In figure 28, the hybrid model with unmodified bifurcation point is compared to the 3-layer SWASH model. The hybrid model although closer to the 3-layer SWASH compared to the 1-layer SWASH, still fails to capture the non-linearity induced by the bar and the additional

viscous dissipation through breaking has a sever effect as wave breaking occurs farther from shore.

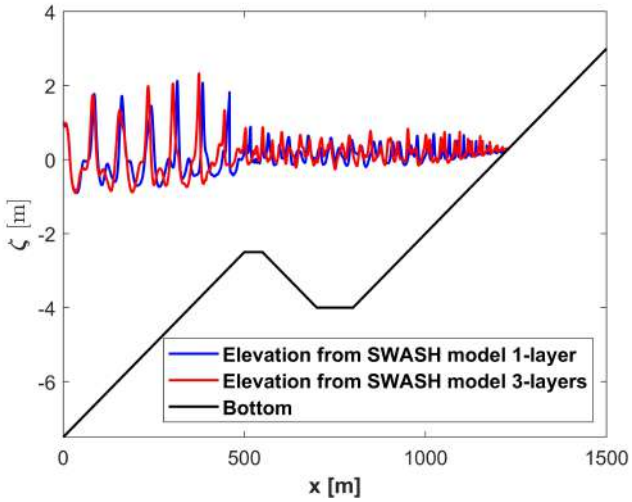


*Figure 27: Comparison of 1-layer SWASH model with 3-layer SWASH.*

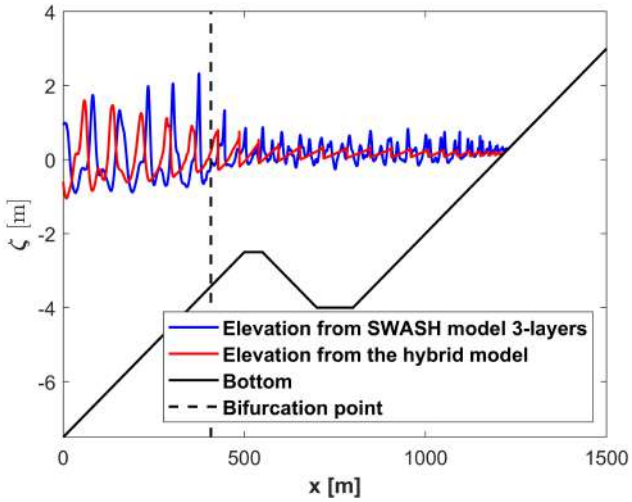


*Figure 28: Comparison of the hybrid model with the SWASH model(3-layer) at the original bifurcation point.*

Therefore, it should be noted that the current parametric bifurcation approach fails to acceptably resolve elevations in case of a bar like bathymetry. Furthermore, given that the selection of the bifurcation point for a linear wave is not particularly clear, the bifurcation depth selection in the case of wave spectra will pose a challenge.

# 5 Conclusions

A hybrid model is developed based on the shallow water equations. Starting with a fully non-hydrostatic system it is gradually reduced to an inertial hydrostatic system as it propagates onto the shore. The results are validated against a single layer SWASH model.

The wave elevations for a monotonic beach slope were demonstrated to agree very well with those from SWASH for waves with low-moderate steepness. There was a slight additional dissipation observed due to different breaking criteria and eddy viscosity in the hybrid model after the bifurcation point. However, there was no significant error in wave set-up. The mean and maximum over-topping fluxes for a range of dikes were compared with SWASH. They were observed to be about half of the values produced by SWASH and was due to the additional dissipation in the model past the bifurcation point. For low discharges the model is found to perform poorly due to the dependence of flows on surface tension and bottom friction near-shore, neither of which are well modelled.

A bar profile is simulated for three different bifurcation points at the depth predicted by the derived parametric model. It is observed that the current parametric bifurcation model does not perform well for bar-like profiles. Overall, the initial model provides good results for linear wave propagation on monotonic beaches and wave over-topping over dikes. The viscous dissipation in the model is higher than that of SWASH. The model also fails to simulate non-linear behaviour observed in highly irregular topographies.

## 5.1 Current model

The developed model is programmed using Python3 a modern programming language in a modular fashion. The language is selected because it allows for easy development and coupling with other hydrodynamic models in the future. At the end of current project, the full model has been programmed for 1D. The breaking, eddy viscosity, and flooding and drying were programmed for 2D alongside the 2D

non-hydrostatic model. Therefore, to complete the current model the 2D pressure Poisson system must be derived and programmed.

The model is being developed as an open source project. Open source means the source code and documents are available to the public and anyone can obtain a copy and modify/develop it. The source code can be accessed at github repository. Github is chosen as it doubles as an open source repository and a version control system.

## 5.2 Future work

In this section, future work recommendations are presented.

The current model has a breaking condition based on linear wave theory. This should be modified to be able to simulate wave spectra. Further, in the case of wave spectra and/or irregular topographies, the identification of the bifurcation point can not be estimated well by the parametric model derived from the wave saturation approach. A thorough study on the effect on the bifurcation in irregular topographies must be conducted.

The current model underestimates over-topping and can be partly attributed to additional dissipation due to the implemented eddy viscosity model. However, as Suzuki *et al.* (2017) suggests semi-empirical equations must be derived to correct for this underestimation as the shallow water equations do not fully resolve the physics responsible for wave over-topping.

A Two-layer non-hydrostatic model without/with minimal use of semi-empirical equations should be developed and verified. The additional computational cost of a second layer should be evaluated against accuracy. Also, parallel processing must be implemented to improve the speed of the model.

# References

Aydin B (2011) *Analytical solutions of shallow-water wave equations*. Ph.D. thesis, Middle East Technical University.

Barnard P, Erikson LH, Foxgrover AC, Hart JAF, Limber P, C OA, van Ormondt M, Vitousek S, Wood N, Hayden MK & Jones JM (2019) Dynamic flood modeling essential to assess the coastal impacts of climate change. *Scientific Reports*, volume 9(1). Article number:4309.

Barthelemy X, Banner ML, Peirson WL, Fedele F, Allis M & Dias F (2018) On a unified breaking onset threshold for gravity waves in deep and intermediate depth water. *Journal of Fluid Mechanics*, volume 841, pages 463–488.

Bates P & De Roo A (2000) A simple raster-based model for flood inundation simulation. *Journal of Hydrology*, volume 236(1-2), pages 54–77.

Bates P, Horritt M & Fewtrell T (2010) A simple inertial formulation of the shallow water equations for efficient two-dimensional flood inundation modelling. *Journal of Hydrology*, volume 387(1-2), pages 33–45.

Battjes JA (1974) Surf similarity. In *Proceedings of 14th Coastal Engineering Conference, Copenhagen, Denmark.*, pages 466–480. American Society of Civil Engineers, New York.

Blayo E & Debreu L (2005) Revisiting open boundary conditions from the point of view of characteristic variables. *Ocean Modelling*, volume 9(3), pages 231–252.

Christou M (2020) Coastal processes. Lecture notes for course CIVE97067, Imperial College London, London.

Costanza A & Carlo LR (2016) A non-hydrostatic pressure distribution solver for the nonlinear shallow water equations over irregular topography. *Advances in Water Resources*, volume 98, pages 47–69.

Courant R, Friedrichs K & Lewy H (1928) Uber die partiellen differenzengleichungen der mathematischen physik. *Mathematische Annalen*, volume 100(1), pages 32 – 74.

de Saint-Venant A (1871) Theorie du mouvement non permanent des eaux, avec

application aux crues des rivieres et a l'introduction de marees dans leurs lits. *Comptes rendus des seances de l'Academie des Sciences*, volume 73, pages 148–154.

Dean RG & Dalrymple RA (1991) *Water wave mechanics for engineers and scientists*, volume 2. World Scientific, singapore. ISBN 9789810204205.

Deltares (2014) *Delft3D-FLOW User Manual*. Deltares, Netherlands, 3.15.34158 edition.

Hunter NM, Bates PD, Horritt MS & Wilson MD (2007) Simple spatially-distributed models for predicting flood inundation. *Geomorphology*, volume 90(3-4), pages 208–225.

Jeschke A, Pedersen GK, Vater S & Behrens J (2017) Depth-averaged non-hydrostatic extension for shallow water equations with quadratic vertical pressure profile: equivalence to boussinesq-type equations. *Numerical methods in fluids*, volume 84(10), pages 569–583.

Karmpadakis I (2020) Coastal processes. Lecture notes for course CIVE97067, Imperial College London, London.

Rijnsdorp D (2011) *Numerical modelling of infragravity waves in coastal regions*. Master's thesis, TU Delft.

Smagorinsky J (1963) General circulation experiments with the primitive equations: I. the basic experiment. *Mon. Wea. Rev.*, volume 91(3), page 99–164.

Stelling G & Zijlema M (2003) An accurate and efficient finite-difference algorithm for non-hydrostatic free-surface flow with application to wave propagation. *International Journal for Numerical Methods in Fluids*, volume 43(1), pages 1–23.

Stockdon HF, Holman RA, Howd PA & Jr SAH (2006) Empirical parameterization of setup, swash, and runup. *Coastal Engineering*, volume 53, page 573–588.

Suzuki T, Altomare C, Veale W, Verwaest T, Trouw K, Troch P & Zijlema M (2017) Efficient and robust wave overtopping estimation for impermeable coastal structures in shallow foreshores using swash. *Coastal Engineering*, volume 122, pages 108–123.

Svendsen IA (2006) *Introduction to nearshore hydrodynamics*, volume 24. World Scientific, singapore. ISBN 9812561420.

Van Engelen TE (2016) *Towards a rapid assessment flood forecasting system for the Southern California coast*. Master's thesis, TU Delft.

Wang W, Martin T, Kamath A & Bihs H (2020) An improved depth-averaged non-hydrostatic shallow water model with quadratic pressure approximation. *Numerical methods in fluids*, volume 92(8), pages 803–824.

Wikipedia, the free encyclopedia (2005) The flooding of new orleans, caused by hurricane katrina in 2005, illustrates the vulnerability of cities that are highly dependent on coastal defenses. [Online; accessed August 13, 2020].

Yamazaki Y, Kowalik Z & Cheung KF (2009) Depth-integrated, non-hydrostatic model for wave breaking and run-up. *International Journal for Numerical Methods in Fluids*, volume 61(5), pages 473 – 497.

Zijlema M, Stelling G & Smit P (2011) Swash: An operational public domain code for simulating wave fields and rapidly varied flows in coastal waters. *Coastal Engineering*, volume 58(10), pages 992–1012.

# A Wave breaking

## A.1 Smagorsinky model

Reynolds averaging of Navier-Stokes leads to Reynolds stresses which is a classic problem and the concept of eddy viscosity was conceived to solve this issue. One of the best know eddy viscosity models is devised by Joseph Smagorinsky(Smagorinsky, 1963). The eddy viscosity is defined as:

$$\nu_h = C_s^2\sqrt{2}\sqrt{(\frac{\partial u}{\partial x})^2 + (\frac{\partial v}{\partial y})^2 + \frac{1}{2}(\frac{\partial u}{\partial x})^2 + \frac{\partial v}{\partial y})^2}\Delta x\Delta y \tag{57}$$

Where, $C_s$ is the Smagorinsky constant and is set as 0.1 for all simulations.

## A.2 Onset of wave breaking

Since the pioneering study on onset of wave breaking, various criteria have been proposed based on idealised theoretical models, laboratory experiments, numerical simulations and field observations. However, given the complexity of the process it is evident that no precise definition or criteria exists for the breaking onset. Briefly they all fall into three categories: geometric, kinematic and energetic criteria. Two different conditions have been implemented in this model.

The first condition is an energetic condition proposed by Barthelemy *et al.* (2018). In this concept, the onset of breaking is viewed as the sheer inability of the waveform to accommodate a local wave energy flux exceeds that in the corresponding maximum recurrent case. A breaking onset threshold parameter **B** is introduced using this concept:

$$B = F/(E||c||) \tag{58}$$

where, F is the local energy flux, E is the local energy density and c is the normalising velocity for the flux ratio. Assuming the free surface pressure as zero the condition in x-direction, reduces to a kinematic criterion at the free surface:

$$B = F_x/(E_x||c||) = u_x/c_x \tag{59}$$

The second condition is based on surf similarity parameter demonstrated by Battjes (1974). This is based on the saturation assumption for waves and the a breaker depth based on wave height is defined as:

$$d_b = \frac{H_b}{\gamma} \tag{60}$$

$$\gamma = 1.16\zeta^{0.22} \sim 0.8 \tag{61}$$

Where, $d_b$ is the depth at which a wave of height $H_b$ breaks. $\gamma$ is called the breaker index. $\zeta$ is the Irribarren number defined as:

$$\zeta = \frac{\beta}{\sqrt{\frac{H_0}{L_0}}} \tag{62}$$

Where, $H_0$ is the deep water wave height, $L_0$ is the deep water wave length and $\beta$ is the slope of the beach.

# B Error definitions in the grid convergence study

## B.1 Analytical solution of a pure standing wave in a half closed basin

This derivation is obtained from Christou (2020).
In the half closed basin, the horizontal velocity at the wall is equal to zero.

$$u = 0 \quad at \quad x = 0 \tag{63}$$

The velocity potential for this wave can be assumed as superimposition of incident and reflected waves based on linear wave theory:

$$\phi = \phi_{incident} + \phi_{reflected} \tag{64}$$

$$\therefore \phi = -\frac{Hg}{2\omega}\frac{\cosh(k(z+d))}{\cosh(kd)}\sin(kx+\omega t) + \frac{Hg}{2\omega}\frac{\cosh(k(z+d))}{\cosh(kd)}\sin(kx-\omega t) \tag{65}$$

$$\therefore \phi = -\frac{Hg}{\omega}\frac{\cosh(k(z+d))}{\cosh(kd)}\cos(kx)\sin(\omega t) \tag{66}$$

From linear wave theory, u at x = 0:

$$u = \frac{\partial \phi}{\partial x} \tag{67}$$

$$\therefore u = \frac{Hkg}{\omega}\frac{\cosh(k(z+d))}{\cosh(kd)}\sin(kx)\sin(\omega t) \tag{68}$$

$$atx = 0 \implies u = 0 \ \ that \ \ satifies \ \ the \ \ condition \ \ at \ \ the \ \ wall$$

The analytical water surface elevation can be obtained from the combined free surface boundary condition:

$$\eta = -\frac{1}{g}\frac{\partial \phi}{\partial t} \text{ at } z = 0 \tag{69}$$

$$\therefore \eta = \frac{H\cosh(k(z+d))}{\cosh(kd)}\cos(kx)\cos(\omega t) \text{ at } z = 0 \tag{70}$$

$$\therefore \eta = H\cos(kx)\cos(\omega t) \tag{71}$$

## B.2 Definition of errors used for studying grid convergence

The errors were estimated for two quantities, the surface elevation and the volume. The RMSE method is used for the surface elevation and is defined as the root of the mean of the error squared at every grid location:

$$RMSE = \sqrt{\frac{1}{N}\sum_{i=1}^{N}\left(\zeta_i - \eta\left(x_i\right)\right)^2} \tag{72}$$

Where, the function $\eta$ is the analytical solution derived in the previous subsection of this appendix. $x_i$ is the $x$ -location and $\zeta_i$ is the elevation at the $i_{th}$ grid point. The volume is estimated by integrating the water depth over the domain:

$$\text{volume} = \int_{x_1}^{x_N} (\eta + d)dx = \int_{x_1}^{x_N} hdx \tag{73}$$

Where, $d$ is the bottom depth. For estimating the volume of the numerical simulations. The water depth $h_i = \zeta_i + d$ is integrated using the trapezoidal numerical integration scheme.

$$\text{volume} = \sum_{i=1}^{N-1} \frac{h_{i+1} + h_i}{2\Delta x} \tag{74}$$

Finally, assuming V as the volume obtained from the simulation and$V_{analytical}$ to be the volume of the analytical solution. The volume error is defined as:

$$volume \;\; error = |1 - \frac{V}{V_{analytical}}| \tag{75}$$